Investigation of global nitrate from the AeroCom Phase III experiment

Huisheng Bian[1,2], Mian Chin[2], Didier A. Hauglustaine[3], Michael Schulz[4], Gunnar Myhre[5,6], Susanne E. Bauer[7,8], Marianne T. Lund[6], Vlassis A. Karydis[9], Tom L. Kucsera[10], Xiaohua Pan[11], Andrea Pozzer[9], Ragnhild B. Skeie[6], Stephen D. Steenrod[10], Kengo Sudo[12], Kostas Tsigaridis[7,8], Alexandra P. Tsimpidi[9], and Svetlana G. Tsyro[4]

[1] Joint Center for Environmental Technology UMBC, Baltimore, MD, USA
[2] Laboratory for Atmospheres, NASA Goddard Space Flight Center, Greenbelt, MD, USA
[3] Laboratoire des Sciences du Climat et de l'Environnement (LSCE), UMR8212, CEA-CNRS-UVSQ, Gif-sur-Yvette, France
[4] Norwegian Meteorological Institute, Blindern, Norway
[5] Department of Geosciences, University of Oslo, Oslo, Norway
[6] Center for International Climate and Environmental Research-Oslo, Oslo, Norway
[7] The Earth Institute, Center for Climate Systems Research, Columbia University, New York, USA
[8] NASA Goddard Institute for Space Studies, New York, USA
[9] Max Planck Institute for Chemistry, 55128 Mainz, Germany
[10] Universities Space Research Association, GESTAR, Columbia, MD, USA
[11] School of Computer, Mathematical and Natural Sciences, Morgan State University, Baltimore, MD, USA
[12] Center for Climate System Research, University of Tokyo, Tokyo, Japan.

Abstract

An assessment of global particulate nitrate and ammonium aerosol based on simulations from nine models participating in the AeroCom Phase III study is presented. A budget analyses was conducted to understand the typical magnitude, distribution, and diversity of the aerosols and their precursors among the models. To gain confidence on model performance, the model results were evaluated with various observations globally, including ground station measurements over North America, Europe, and East Asia for tracer concentrations and dry and wet depositions, as well as with aircraft measurements in the Northern Hemisphere mid-high latitudes for tracer vertical distributions. Given the unique chemical and physical features of the nitrate occurrence, we further investigated the similarity and differentiation among the models by examining: 1) the pH-dependent NH_3 wet deposition; 2) the nitrate formation via heterogeneous chemistry on the surface of dust and sea-salt particles; and 3) the nitrate coarse mode fraction (i.e., coarse/total). It is found that HNO_3, which is simulated explicitly based on full O_3-HO_x-NO_x-aerosol chemistry by all models, differs by up to a factor of 9 among the models in its global tropospheric burden. This partially contributes to a large difference in NO_3^-, whose atmospheric burden differs by up to a factor of 13. The atmospheric burdens of NH_3 and NH_4^+ differ by 17 and 4, respectively. Analyses at the process level show that the large diversity in atmospheric burdens of NO_3^-, NH_3, and NH_4^+ is also related to deposition processes. Wet deposition seems to be the dominant process in determining the diversity in NH_3 and NH_4^+ lifetimes. It is critical to correctly account for contributions of heterogeneous chemical production of nitrate on dust and sea-salt, because this process overwhelmingly controls atmospheric nitrate production (typically >80%) and determines the coarse and fine mode distribution of nitrate aerosol.

1. Introduction

Atmospheric aerosols adversely affect human health and play an important role in changing the Earth's climate. A series of multimodel studies have been coordinated by

the international activity of Aerosol Comparisons between Observations and Models (AeroCom) in its Phase I and II model experiments that have systematically assessed the presence and influence of almost all major atmospheric anthropogenic and natural aerosols (such as sulfate, dust, and carbonaceous aerosols) (e.g., Kinne et al., 2006; Schulz et al., 2006; Textor et al., 2006; Koch et al., 2009; Huneeus et al., 2011; Tsigaridis et al., 2014; Kim et al., 2015). Very little attention has been drawn to nitrate aerosol (hereafter "nitrate" referring to particulate nitrate unless otherwise specified) other than its contribution to radiative forcing (Myhre et al., 2013). One obvious reason is that not many models used to include nitrate owing to the chemical complexity of nitrate formation. However, atmospheric nitrate aerosol not only exerts direct effects on air quality and climate, but also uniquely impacts the Earth system by being directly involved in tropospheric chemistry and constraining net primary productivity, hence altering carbon sequestration and ecological effects, via its deposition (Prentice et al., 2001).

Atmospheric nitrate contributes notably to total aerosol mass in the present-day, especially in urban areas and agriculture regions. Nitrate is about a quarter of sulfate in terms of overall global burden, AOD, and direct forcing at the present-day according to the study of AeroCom II direct forcing experiment (Myhre et al., 2013). This conclusion is confirmed by recent publications using various individual models and emission inventories (Bellouin et al; 2011; Bauer et al., 2007; Hauglustaine 2014; Karydis et al., 2016; Mezuman et al., 2016; Paulot et al., 2016). Regionally, considerable evidences from in-situ measurements (Bessagnet et al., 2014; Haywood et al., 2008; Jimenez et al., 2009; Malm et al., 1994; Vieno et al., 2016) and model results (Karydis et al., 2011; Ensberg et al., 2013; Trump et al., 2015) indicate that nitrate becomes one of the major aerosol species in urban and agriculture environments. For example, nitrate concentration is about half of sulfate during the summer season in Beijing (Zhou et al., 2016) and represents a large portion of wintertime aerosol mass in the San Joaquin Valley in California (Pusede et al., 2016).

More importantly, the importance of aerosol nitrate is likely to increase over the century with a projected decline in SO_2 and NO_x emissions and increase in NH_3 emissions (IPCC, 2013). With the reduction of SO_2 emissions, less atmospheric NH_3 is required to neutralize the strong acid H_2SO_4. The excess of NH_3 results in gaseous HNO_3 and NH_3 entering the condensed phase, and their subsequent dissociation yields nitrate and ammonium ions. The trend of future nitrate depends on which is the limited species, NO_x or NH_3, for nitrate formation (Tsimpidi et al., 2007; 2008). Generally, our atmosphere, at its current and foreseeable near future, is still in an NH_3-limited condition according to sensitivity studies by Heald et al. (2012) and Walker et al. (2012). Almost all global models predicted an overall increase of atmospheric nitrate burden during this century based on current available emission inventories (Bauer et al 2007; 2016; Bellouin et al., 2011; Hauglustaine et al., 2014; Li et al., 2014). For example, using CMIP5 future emission projections, Bellouin et al. (2011) concluded that, by 2090, nitrate would become an important aerosol species in Europe and Asia, contributing up to two thirds of the globally averaged anthropogenic optical depth. However, the predicted trend of surface nitrate is mixed. Some studies estimated a consistent increase of surface nitrate

(Bellouin et al., 2011), while others pointed out that this increase might vanish or even reverse over some regional urban areas due to the decline of NO_x emissions (Bauer et al., 2016; Pusede et al., 2016; Trail et al., 2014). Nevertheless, the potentially increasing importance of nitrate in climate and its large uncertainty in future surface nitrate predictions urge us to characterize model performance and understand the physicochemical mechanisms behind the diversity of nitrate simulations.

Nitrate is also important in that its formation directly affects tropospheric chemistry. First, the formation of nitrate, through either aqueous phase chemical reaction between HNO_3 and NH_3 (Metzger et al., 2002; Kim et al., 1993) or heterogeneous reaction of nitrogen species such as HNO_3, NO_3, and N_2O_5 on the surface of dust and sea salt aerosol particles (Bauer et al., 2004; 2005; Bian et al., 2003; Dentener 1996; Liao et al., 2003), converts gas phase nitrogen species into aerosols. Consequently, the global tropospheric NO_x concentration and the rate of conversion of N_2O_5 to HNO_3 will be reduced (Riemer et al., 2003), which in turn leads to the reduction of atmospheric oxidants. For example, global tropospheric O_3 can be reduced by 5% (Bauer et al., 2007) and tropical Atlantic OH by 10% (Bian et al., 2003) just through the heterogeneous reactions of nitrogen radicals on dust. Second, the most important removal path for nitrogen from the atmosphere is the formation of HNO_3, which is subsequently deposited (Riemer et al., 2003). Since HNO_3 is subject to partitioning between the gas and aerosol phases, the lifetimes of nitrogen species can be shortened by the formation of tropospheric nitrate aerosol because the loss of total HNO_3 will be accelerated by a much higher dry deposition in the aerosol phase.

Large nitrogen deposition occurs over both land and ocean (Dentener et al., 2006; Kanakidou et al., 2012; 2016). Nitrogen deposition can either benefit or impair ecosystem productivity depending on the initial balance of nutrients since different ecosystems have different Nr (reactive nitrogen) availability and retention (Galloway et al., 2004; Prentice et al., 2001). If fixed Nr is deposited as nitrate in forests, it may act as a "fertilizer," stimulating growth and thus enhancing carbon sequestration (Fowler et al., 2015). But when the accumulated deposition exceeds the nutritional needs of the ecosystem, nitrogen saturation may result (Fenn et al., 1996). Soil fertility declines due to the leeching of cations (Milegroet and Cole, 1984) and, thus, carbon uptake diminishes. The balance between fertilization and saturation depends on the spatial and temporal extent of nitrogen deposition. In order to determine the extent to which the emissions of air pollutants will have to be reduced and whether the environment needs to be protected from damage, it is essential to know where and by how much N deposition exceeds nature's tolerance (Dentener et al. 2006; Lamarque et al., 2005; Phoenix et al., 2006).

Here we present a nitrate-focused study that has been organized as a part of the series of AeroCom phase III experiments (https://wiki.met.no/aerocom/phase3-experiments). The goals of this activity are to (1) address the diversity of the nitrate simulation by the AeroCom multi-models and diagnose the driving processes for the diversity, (2) explore the uncertainty of the model nitrate simulations constrained against various measurements from ground station networks and aircraft campaigns, and (3) investigate how the formation of nitrate changes in different models in response to perturbation on

key precursors and factors that determine nitrate formation. We focus on the first two objectives in this paper. Such a study directs us on how to improve the representation of nitrate aerosol formation and size distribution in climate chemistry models and reveals nitrate effects on global air quality and climate.

Building upon the analysis of the multi-model diversity, three additional sensitivity experiments are designed using the GMI model to further explore the potential sources for the diversity on physical and chemical process-level. First, we explore the impact of pH-dependent NH_3 wet deposition on atmospheric NH_3 and associated nitrogen species. We then reveal the importance of mineral dust and sea salt in the nitrate formation and check the resultant nitrate aerosol size distribution that is particularly important in nitrate forcing estimation.

The paper is organized as follows. Section 2 introduces the experiment setup including the emission inventories used and the participating Aerocom models. Observations of surface tracer concentrations and dry and wet depositions over U.S., Europe, and East Asia, as well as aircraft measurements in the ARCTAS campaigns are described in section 3. We present AeroCom model inter-comparison and the model evaluation using aforementioned observations in section 4. Based on the knowledge from previous sections, we further discuss nitrate formation in response to physiochemical methodologies in section 5 and summarize our major findings in section 6.

2. Experiment setup and AeroCom model description

2.1 Experiment setup

The AeroCom III nitrate experiment comprises one baseline and six perturbation simulations, with the latter designed for assessing the possible future changes of emission and meteorological fields relevant to nitrate formation. Models are advised to use the same prescribed emission datasets for gases and aerosols. Emissions from anthropogenic, aircraft, and ship for aerosol and ozone simulations are obtained from the recently developed HTAP v2 database (Janssens-Maenhout et al., 2015) that provides high spatial resolution monthly emission. For the tracers that are included in ozone chemistry but are not provided by HTAP v2 (i.e. some volatile organic compounds), they should be obtained from CMIP5 RCP85 with a linear interpolation between 2005 and 2010. Biomass burning emissions are the emissions of GFED3 (Werf et al., 2010) in 2008 [http://www.globalfiredata.org/data.html]. The NH_3 emission from ocean is adopted based on the compilation of GEIA emission inventory [Bouwman et al., 1997]. Participating modeling groups use their own emissions of dimenthyl sulfide (DMS), dust, sea salt, and NO from lightning, since they are calculated based on models' meteorological fields.

A full year simulation for 2008 is required for the nitrate model experiment. There are several in-situ observation datasets available in 2008 for model evaluation, including the surface concentration and deposition measurements over the US (CastNet, AMoN, NDAP/NTN), Europe (EMEP), and Asia (EANET), and the aircraft measurements of vertical profiles (e.g. ARCTAS-A, ARCTAS-CARB, and ARCTAS-B). All participating

models are required to use the reanalysis or nudged meteorological data for 2008 and allow one-year spin up for the baseline simulation.

2.2 AeroCom models

Nine models participate in the AeroCom III nitrate experiment. Their general nitrate-related physiochemical mechanisms are summarized in Table 1. Further detailed information on their thermodynamic equilibrium model (TEQM) is given in Table 2.

The models participating in this study are divided into two groups. Group one (CHASER, EMAC, INCA, GISS-MATRIX, and GISS-OMA) run chemical fields together with meteorological fields, while group two (EMEP, GMI, OsloCTM2, and OsloCTM3) simulate chemical fields using archived meteorological fields. Most models in this study have a horizontal resolution around 2-3 degrees except EMEP with 0.5 degree. Vertically, most models cover both the troposphere and the stratosphere with a peak altitude up to 0.01 hPa except EMEP that extends vertically up to 100 hPa into the troposphere only.

All models use full gas phase O_3-NO_x-HO_x chemistry to produce HNO_3 and consider the feedback of nitrate aerosol formation on HNO_3 calculation. However, due to the complexity of chemical mechanisms for organic nitrate compounds and different recommendations for reaction rates, HNO_3 fields produced by the models differ greatly. This difference propagates into the subsequent gas-aerosol reactions for nitrate formation.

These models are very different in their approaches on gas-aerosol reactions in nitrate formation. All models consider reactions between NH_3 and HNO_3. However, models differ dramatically in whether to include heterogeneous reactions on dust and sea salt (Table 1). Some account for both, some for only dust or sea salt, and some do not account for any of them at all. The methods used by the models in accounting for NH_3 and dust/sea salt contributions are also different. Please also note that the heterogeneous chemical production of nitrate mentioned in this paper refers only the reaction of HNO_3 on dust and sea salt particles. A series of reactions, such as N_2O_5 hydrolysis and $BrONO_2$ hydrolysis, affect HNO_3 simulation. These reactions are typically considered in O_3-NO_x-HO_x chemistry and their discussion is beyond the scope of this paper.

All participating models adopt TEQM to deal with aqueous and solid phase reactions and gas-aerosol partitioning (Tables 1 and 2). This is based on the assumption that volatile species in the gas and aerosol phases are generally in chemical equilibrium. However, the assumption is not always warranted in some cases, as we will discuss in section 5.2. Even with the TEQM approach, nitrate calculation could differ due to treatments of equilibrium constants or chemical potentials, solute activity coefficients, water activity, and relative humidity of deliquescence (RHD). The parameterizations adopted by the models to deal with multicomponent activity coefficient, binary activity coefficient, and water activity are given in table 2. GISS-OMA, Oslo-CTM2 and Oslo-CTM3 are special in that they assume aerosols to be metastable so that the model does not take into account formation of solids in this study. All other models do consider the effect of the hysteresis

of particle phase transitions. All models also assume that the overall particles are large enough to neglect the Kelvin effect.

The participating models call the TEQMs in different ways to account for aerosol size effect. All the TEQMs (ISORROPIA-I, ISORROPIA-II, MARS, RPMIRES, INCA, and EQSAM3) assume particles to be internally mixed, i.e. all particles of the same size have the same composition. However, some parent models (CHASER, EMEP, GMI, INCA, GISS-MATRIX and GISS-OMA) call their TEQMs only once for fine mode aerosol particles, while the others (EMAC, OsloCTM2 and OsloCTM3) call their TEQMs from different aerosol size bins. For example, Oslo-CTM2 and Oslo-CTM3 consider a bi-modal aerosol size-spectrum with two major aerosol modes, fine and coarse, and calculate gas-aerosol equilibrium partitioning with EQSAM3 first for fine mode and then for coarse mode. Additionally, to account for kinetic limitations, EMAC calculates the phase partitioning in two stages. In the first stage, the amount of the gas-phase species that is able to kinetically condense onto the aerosol phase within the model time step is calculated, while in the second stage, the TEQM redistributes the mass between the two phases assuming instant equilibrium (Pringle et al., 2010).

The TEQMs also differ in the chemical components considered. Specifically, the TEQMs in CHASE, EMEP, GISS-MATRIX, GISS-OMA, GMI and INCA include only species of sulfate, nitrate, ammonium and their gas, liquid, and solid components. The models Oslo-CTM2 and Oslo-CTM3 add NaCl and HCl, while the model EMAC further expands the species by including dust-related crustal material such as Ca^{2+}, K^{+}, and Mg^{2+}.

These TEQMs differ in their computational approaches as well. Computational efficiency is a prime consideration for a TEQM that is designed for incorporation into a global air quality and climate study. To speed up the calculation, TEQMs typically divide the system into sub-domains based on RH and concentrations of ammonium, sodium, crustal cations, and sulfate. Corresponding approximation could be adopted for each sub-domain with the minimum numbers of equilibriums and unknown components. As listed in table 2, the numbers of sub-domains are 4, 5, 4, 2, 3, and 3 for the TEQM ISORROPIA-I, ISORROPIA-II, MARS, RPMIRES, INCA, and EQSAM3, respectively.

The ways to account for the contribution of dust and sea salt to nitrate formation are also different. Some models (EMAC, Oslo-CTM3, and Oslo-CTM2) include dust and/or sea salt components in their TEQM models directly, while some models (EMEP, GISS-OMA, GMI, and INCA) use an approach of first order loss rate outside their TEQMs to account for the heterogeneous reactions of HNO_3 on the surface of dust and sea salt. For the latter approach, the gamma rates and their RH dependence adopted by the models differ as well.

Dry and wet deposition of NH_3, ammonium nitrate, and ammonium sulfate are treated similarly to other gas and aerosol tracers in the models. It is worth pointing out that there is a different consideration for Henry's law constant of NH_3 used by the models. Some models modify it based on the pH value of cloud water while others do not. We will discuss the impact of these two treatments on nitrate simulation in section 5.1.

We introduce only the major characteristics of thermodynamic equilibrium models since this study aims for the evaluation and explanation of overall nitrate diversity among the GCM/CTM models from all potential aspects. The detailed discussion of the models chemical mechanism of gas phase reactions and the aerosol optical properties adopted by the models is also beyond this work. Readers could refer to the references listed in Tables 1 and 2 for any further details.

3. Observations

We use surface measurements from ground station networks and aircraft campaigns to evaluate modeled surface concentrations, dry and wet depositions, and vertical distributions of nitrate and related species (Table 3).

3.1 Surface measurements of concentrations and deposition rates

Ambient concentrations of sulfur and nitrogen species throughout the US and Canada have been measured by the ground station network CASTNET (Clean Air Status and Trends Network) (Figure 1). The measurements use a 3-stage filter pack with a controlled flow rate. The measurements of CASTNET do not include NH_3. AMoN (Ammonia Monitoring Network), measuring concentrations of ambient NH_3, has been deployed at CASTNET sites starting from October 2007 using passive samplers. The corresponding tracers' surface concentration measurements over Europe have been conducted by EMEP (The European Monitoring and Evaluation Programme). The measured sites of all these networks are located in rural areas or sensitive ecosystems, representing a larger region by avoiding influences and contamination from local sources. Surface concentrations over East Asia are inferred from the measurement of dry deposition by EANET (Acid Deposition Monitoring Network in East Asia). This network provides acid deposition from a regional monitoring network including 13 countries in East Asia using standardized monitoring methods and analytical techniques.

CASTNET also provides dry deposition of sulfate and nitrogen species. Direct measurements of dry deposition fluxes (D) are expensive so D is calculated as the measured pollutant concentration (C) multiplied by the modeled dry deposition velocity (V_d). V_d is either estimated by the Multi-Layer Model fed with measured hourly meteorological data or derived from historical average V_d for sites with discontinued meteorological parameters.

Direct measurements of wet deposition fluxes of sulfate, nitrate, and other ions have also been performed by NADP/NTN (the National Atmospheric Deposition Program / National Trends Network) across the contiguous US, Canada, Alaska, and the US Virgin Islands and EANET over East Asia. Sites are predominantly located away from urban areas and point sources of pollution. Each site has a precipitation chemistry collector and gauge. Both networks can measure wet deposition for a continuous period (weekly for NADP/NTN and daily for EANET), or every precipitation event if using an automated collector (wet-only sampling).

Data is quality assured for all measurements. Measurements over North America use automated screening techniques, semi-annual calibration results, site operator comments, and manual data review. Quality assurance of EMEP is carried out on both the national level and by the Chemical Co-ordinating Centre (CCC). The quality of EMEP measurements is not equal at the national level (Schaap et al., 2002; 2004). Sites in North, Western and Central Europe were generally well equipped and performing, while sites in the rest of Europe suffered from inadequate sampling and calibrating methods due to political and/or economical reasons. The quality of ammonia measurement is relatively low since some laboratories experienced contamination problems (Williams et al., 1992). Although EANET adopts standardized monitoring methods and analytical techniques, quality assurance is carried out on the national level.

3.2 Aircraft measurements of vertical profiles

Aircraft campaign measurements during the 2008 Arctic Research of the Composition of the Troposphere from Aircraft and Satellites (ARCTAS) are used to evaluate tracer vertical distribution simulated by the models (Bian et al., 2013; Jacob et al., 2010). Three phases of the campaign, ranging from Northern Hemisphere mid-latitude industrial region (ARCTAS-CARB, June 2008) to high latitude Arctic regions influenced by long-rang pollution transport (ARCTAS-A, April 2008) and by local boreal biomass burning (ARCTAS-B, July 2008), provide well encompassing environment observations. All flights were conducted by the NASA DC-8 aircraft and the flight tracks of these three phases are presented in Figure 2. An onboard HR-ToF-AMS instrument (Cubison et al., 2011; DeCarlo et al, 2006) measured fine mode aerosol concentrations (PM1) along the fight track including NO_3^-, NH_4^+, and SO_4^{2-} at STP conditions (1013mb and 273.15K) at a sampling time interval of ~12 seconds. Accuracy estimate of 2-standard deviations, likely conservative, is 34% for inorganics, dominated by the uncertainty in particle collection efficiency due to particle bouncing (Huffman et al., 2005).

4. Model intercomparison and evaluation

4.1 AeroCom model inter-comparisons of global distributions and budgets

4.1.1 NH_3 and NH_4^+

Six models use HTAP2 anthropogenic emissions, two (GISS-MATRIX and GISS-OMA) use CMIP5 emissions, and one (INCA) uses ECLIPSE emissions. Table 4b shows that eight models have the annual NH_3 emission values within 5% of the value from the AeroCom experiment recommended emission inventories, but INCA is 11% higher. The similar emission distributions ensure that the examined inter-model diversities are truly caused by the differences in physicochemical processes among the models. The normalized root-mean-square deviation (NRMSD) of NH_3 global burden among models is 1.17 and 0.33 with and without EMAC included. This drastic change in global burden NRMSD by EMAC is caused by its special treatment of wet deposition. In fact, the removal of trace gases and aerosol particles by clouds and precipitation in EMAC is not calculated based on empirically determined, fixed scavenging coefficients, but rather by solving a system of coupled ordinary differential equations, explicitly describing the processes involved (Tost et al., 2006). This method resolves feedback mechanisms between the multi-phase chemistry and transport processes involved. The liquid phase

reaction set used converts all the scavenged NH_3 (or HNO_3) into NH_4^+ (or NO_3^-) in the liquid phase so that at the end everything that is deposited is the total NH_4^+ and NH_3.

Atmospheric NH_4^+ is produced entirely by NH_3 chemical transformation. The models simulate NH_4^+ much closer in chemical production (difference less than a factor of 2) than in lifetime (difference up to a factor of 5.2), indicating removing rates are a key factor in controlling the global burden of NH_4^+. For example, CHASER has a much longer lifetime of NH_4^+ (i.e. 9.8 days versus 4.3 days in average), which indicates a slow deposition removal of NH_4^+ from the atmosphere. Consequently, CHASER simulates a much higher atmospheric NH_4^+ burden than other models.

4.1.2 HNO_3 and NO_3^-

HNO_3, an important nitrate precursor, differs by up to a factor of 9 in its global tropospheric burden among the models (Table 4c). All models simulated HNO_3 based on a full gas phase O_3-HO_x-NO_x chemistry and coupled it with aerosol chemistry. This HNO_3 diversity will naturally be propagated into the NO_3^- simulation. However, further discussion of the detailed consideration of full gas-aerosol chemistry for HNO_3 diversity among the models is beyond the scope of this study.

The resultant aerosol product (i.e., NO_3^-) does not entirely follow its precursor (i.e., HNO_3) in terms of global burden: EMEP has very low HNO_3 but high NO_3^-, two GISS models (MATRIX and OMA) simulate high HNO_3 but low NO_3^-, while OsloCTM3 has an average HNO_3 but more than triple high NO_3^- than average (Tables 4a and 4c). Furthermore, the difference in NO_3^- global burden (up to a factor of 13) is larger than that of HNO_3. Differences in chemical mechanisms of NO_3^- production could be a potential explanation along with the difference in HNO_3 precursor. Unfortunately, only GMI and INCA provide a detailed NO_3^- chemistry budget analysis. Nevertheless, we can infer that the total chemical production of NO_3^- must be very low (~ 10Tg) in the two GISS models while very high (> 100 Tg) in OsloCTM2 and OsloCTM3 based on the reported total NO_3^- loss. Combining this information with the HNO_3 global tropospheric burden (Table 4c), we can further infer that the chemical conversion from HNO_3 to NO_3^- must be lowest in the two GISS models while highest in the two Oslo models. Several factors could influence this conversion, such as the availability of alkaline species of mineral dust and sea-salt particles and the physicochemical mechanism of nitrate formation on dust and sea-salt, availability of NH_3 after combining with SO_4^{2-}, and the atmospheric meteorological fields of temperature and relative humidity. More discussions are given in sections 5.2 and 5.3.

Atmospheric lifetime of NO_3^- differs up to a factor of 4, from about 2 days in GMI and OsloCTM2 to larger than 7 days in GISS-OMA and GISS-MATRIX. The slower removal processes in the two GISS models compensate the low chemical production and help to maintain their NO_3^- atmospheric burden (Figure 3 and Table 4a).

4.2 Model-observation comparisons

4.2.1 Comparisons of surface concentrations over North America, Europe, and East Asia

Understanding diversity among model simulations and potential physiochemical processes behind the difference is important but not sufficient. The information has to be combined with the knowledge of model performance obtained directly from comparisons, particularly down to processes level, against various measurements to gain a direction of any improvement. Figures 4a-c show a model-observation comparison for surface mass/volume mixing ratios of NO_3^-, NH_4^+, NH_3, HNO_3, and SO_4^{2-} over North America (CastNET), Europe (EMEP), and East Asia (EANET). Each point represents a monthly mean concentration at one observational site. Generally, the agreement between model and observation is better for aerosol components than for gas tracers (i.e. the precursor species NH_3 and HNO_3) over all three regions. All models underestimate NH_3 surface volume mixing ratio with a ratio of model to observation down to 0.14, while most models overestimate surface HNO_3 volume mixing ratio with a ratio up to 3.9 over North America. The worse performances of NH_3 against observations may be also associated to their relatively lower measurement accuracy, i.e. easier to be contaminated during measurement (Williams et al., 1992). Among aerosol simulations, model performance is very similar for NH_4^+ and SO_4^{2-}, while slightly worse for NO_3^- that is dispersed further away from the 1:1 line, particularly at low NO_3^- values. The NO_3^- simulation over East Asia is worst with the average normalized root mean square to be 1.3 and 1.8 higher than that over North America and Europe, respectively.

4.2.2 Comparisons of vertical profiles with aircraft measurements during the ARCTAS field campaign

Evaluation of model performance presented in 4.2.1 for the surface concentrations in the source regions is highly dependent on the accuracy of the emission inventory. On the other hand, evaluation using aircraft measurements, particularly over remote regions, provides further examination of models' physicochemical evolution during transport. Here we use data from three phases of the ARCTAS aircraft campaign (section 3), and the results are shown in Figure 5. All model results of NO_3^-, NH_4^+, and SO_4^{2-} are sampled along flight track and averaged regionally within 1km vertically for each campaign phase before comparing with the corresponding aircraft measurements. Note that only EMAC, EMEP and GMI report daily 3D global tracer concentrations, while the others report monthly only. Note also that only EMEP and GMI adopt daily biomass burning emission while the others use monthly emission. To verify the representativeness of monthly mean concentration in capturing the main features exhibited in model-observation comparisons, daily and monthly concentrations of the three models are used in the same spatial sampling to compare with the measurements (see the green lines for daily and red for monthly in the figure). The comparison keeps its main features as shown when using both daily and monthly model data.

During ARCTAS-A, which was conducted in April 2008 and was based in Fairbanks, Alaska, none of the models captures the long-range transport of aerosols primarily from Asia, which enter Polar Regions at altitudes between 2-7 km (Fig. 3 in Bian et al., 2013). Except CHASER and EMAC, all models also report a significant underestimation of NH_4^+ and SO_4^{2-} in boundary layer. A previous assessment of pollution transport to the

Arctic indicated that aerosol wet removal plays an important role in the uncertainty of Arctic aerosols (Shindell et al., 2008). Another potential reason is that some large fire activities in Siberia during April 2008 (Jacob et al., 2010) may be missed in the GFED3 emission inventory. The underestimation of SO_4^{2-} may help bring up NO_3^- production, particularly at high altitudes. During ARCTAS-CARB, which was conducted in June 2008 based in Palmdale, California, agreement between model and measurements is much improved. Almost all models show a rapid vertical decease from surface to free troposphere, which is consistent with the measurements of SO_4^{2-} and NH_4^+, but not NO_3^-. The observation shows a maximum of NO_3^- at about 1.5 km, which is not represented by any of the models. During ARCTAS-B, which was conducted in July 2008 and was based in Cold Lake, Canada, when there were frequent local wild fires, model performances are mixed. In general, most models underestimate concentrations of NO_3^-, NH_4^+ and SO_4^{2-}below 4 km. CHASER model is special in that it overestimates SO_4^{2-} significantly. This may be contributed to high (near surface) to comparable (free troposphere) model simulation of NH_4^+ but an underestimation of NO_3^-. Different from other models, the INCA model shows an enhancement of pollutants in the upper troposphere with concentrations much higher (more than 5 times) than observations. This behavior may be derived from a much vigorous vertical uplifting to the upper troposphere as revealed from Fig. 3a-3b combined with a low NH_3 Henry's law constant used by INCA, see discussion in section 5.2.

Note that all measurements and model data we discussed above are for fine mode aerosols. Total NO_3^- (orange line using monthly model output) is also shown in the figure to reveal whether a changing of partitioning of fine and coarse mode NO_3^- could improve the model-observation comparison. It seems that the new version of OsloCTM3 may put too much of NO_3^- in coarse mode.

4.3 Model-observation comparison for dry and wet deposition

4.3.1 Dry deposition

The budget analyses in section 4.1 concluded that dry and/or wet depositions are most likely the main processes driving the diversity in the model simulations. Thus, further evaluation of deposition processes is needed to identify any potential problematic model.

The dry depositions of NO_3^-, NH_4^+, HNO_3, and SO_4^{2-} simulated by the models are compared against CASTNET measurements over North America (Figure 6). Generally, the overestimation of surface HNO_3 concentrations (Figure 3a) results in the higher dry depositions of HNO_3, but this is not the case for NO_3^-. Meanwhile, most of the models give a better dry deposition simulation for aerosol SO_4^{2-} and NH_4^+ than for aerosol NO_3^-, except CHASER. Specifically, GISS-OMA and GISS-MATRIX have wide spread dry NO_3^- deposition at any given measurement value. In other words, the two models underestimate NO_3^- dry deposition significantly at many observational stations, which does not occur in the other models. This low dry deposition simulation may occur outside North America as well because the global dry depositions of the two models are lower than others (Table 4a). OsloCTM2 overestimates NO_3^- dry deposition significantly, which is probably linked to its larger coarse fraction of the nitrate aerosol (see discussion in

section 5.3). OsloCTM3 improved its dry deposition scheme although the model still overestimates the dry deposition. We will discuss the OsloCTM2 NO_3^- simulation over North America by combining the model's wet deposition in the next section. NH_4^+ dry deposition is low in GMI but very high in CHASER. This performance is also extended globally as summarized in Table 4b.

4.3.2 Wet deposition

The wet deposition simulations from the nine models are compared with surface measurement over North America (Figure 7a) and East Asia (Figure 7b) for oxidized NO_3^- (i.e. total NO_3^- and HNO_3), total NH_4^+ and NH_3 (tNH_4^+), and SO_4^{2-}. All models tend to underestimate the wet deposition of tNH_4^+ and SO_4^{2-} over the two regions. Models EMAC, GMI, OsloCTM2 and OsloCTM3 have relatively high wet removal for oxidized NO_3^-, while EMEP removes much less than others over North America. All models' wet deposition of oxidized NO_3^- is biased low over East Asia. As we discussed above, OsloCTM2 and OsloCTM3 have very high dry NO_3^- depositions (Figure 6) compared with CASTNET observations. The overall high dry and wet NO_3^- depositions along with high atmospheric concentrations (Figure 4a) indicate that the chemical formation of NO_3^- in the two models must be also high. This performance might be also true on global scale since the inferred chemical productions of NO_3^- in the two models are the highest (Table 4a). CHASER has the lowest tNH_4^+ wet deposition. This may result in a very high NH_4^+ dry deposition (Figure 6) and concentration (Figures 4a-c, 5) compared with observations and other models. Overall, wet deposition seems to be the dominant process in determining the diversity in NH_3 and NH_4^+ lifetime (Table 4b).

Note that we use the traditional approach of comparing models' grid box mean values with observations, which does not take into account the impact of the models' horizontal resolutions in their representation of observations (Schutgens et al., 2016). Since majority models (except EMEP) have horizontal resolutions around 2-3 degrees, the models grid box means tend to smooth out extreme (i.e. very low or high) observations. Consequently, the slopes of the fitting lines are generally less than 1 on the scattering plots with model as y-axis and observation as x-axis (e.g. Figures 4a-d, 6, 7a-b).

5. Discussion of major uncertainties in nitrate formation

Large uncertainties of nitrate studies result from the complexity of the simulations which must consider a comprehensive NO_x-NMHC-O_3-NH_3 chemistry and a thermodynamic equilibrium model (TEQM) to partition semi-volatile ammonium nitrate between the gas and aerosol phases. Nitrate aerosol concentrations depend on temperature, relative humidity (RH), and concentrations of HNO_3, NH_3, NH_4^+, SO_4^{2-}, Cl^-, Na^+, Ca^{2+}, K^+, Mg^{2+}, organic acids, among others. A further complicating factor is that the equilibrium for the coarse mode is somewhat questionable (Feng and Penner, 2007). In addition, wet removal of NH_3 is very sensitive to the pH in cloud water. We will discuss some of these uncertainties below.

5.1 pH-dependent NH_3 wet deposition

Gas tracer NH_3, a precursor of ammonium aerosol, experiences atmospheric wet deposition and its deposition rate is typically calculated using Henry's Law. Henry's law

553 constant (H) of gases in water is usually given at 298 K (indicated by Θ in superscript)
554 and can be adjusted by temperature (T).

$$H(T) = H^{\Theta} * \exp\left(-\frac{\Delta H_{sol}}{R}\left(\frac{1}{T} - \frac{1}{T^{\Theta}}\right)\right) \quad (1)$$

555 Here ΔH_{sol} is the enthalpy of dissolution and R is the gas constant.
556
557 For some acidic/basic gases, including NH_3, Henry's law constant is also a function of
558 pH in cloud water (a.k.a effective Henry's law constant H^{Θ^*}). As explained in the
559 Appendix, the H^{Θ^*} is inferred from H^{Θ} with a correction of pH (pH = $-\log_{10}[H^+]$) as

$$H^{\Theta^*} = H^{\Theta}\frac{K_{al}[H^+]}{K_w} \quad (5)$$

560 Here, $K_{al} \approx 1.8\text{x}10^{-5}$ and $K_w = 1.0\text{x}10^{-14}$ at 298 K in pure water (see Appendix). However,
561 not every model accounts for pH adjustment (i.e. the reaction of equation 2 in Appendix)
562 for NH_3 dissolution. More accurately, the EMAC model implicitly calculates the
563 effective Henry's law constant by solving a set of partial differential equations, which
564 includes not only the gas-liquid phase equilibria, but also the reactions in the liquid phase
565 (i.e. dissociation or acid-base equilibria, Redox reactions and photolysis reactions in the
566 liquid phase, see Tost et al.(2006)). Therefore, the gas-liquid phase equilibrium is
567 explicitly calculated based on the chemical mechanism used in the liquid phase. As listed
568 in Table 5, the rest of the models are generally divided into two groups based on their
569 effective Henry's law constant: (1) INCA, GISS-OMA and GISS-MATRIX has $H^{\Theta^*} \leq$
570 100 (L-theta without pH correction) and (2) CHASER, GMI, OsloCTM2 and Oslo-
571 CTM3 has $H^{\Theta^*} > 10^{+5}$ (H-theta with pH correction). The NH_3's H^{Θ^*} adopted by the
572 models varies dramatically, up to an order of 6 in magnitude among all the models and a
573 factor of 10 just for the models in H-theta group (Table 5). The latter corresponds to a
574 range of pH from 4.5 (Oslo-CTM2) to 5.5 (CHASER).
575
576 To examine how sensitive of NH_3, NH_4^+ and NO_3^- simulations in response to the
577 magnitude of NH_3's H^{Θ^*}, we performed a sensitivity experiment, named TWET, in the
578 GMI model in which there was no pH adjustment for NH_3 Henry's law constant (i.e.
579 H^{Θ^*}=61 instead of 1.05e+6, see table 6). The resultant annual budgets of dry/wet
580 deposition, chemistry production and loss, and atmospheric loading of NH_3,
581 NH_4^+ and NO_3^- are summarized in Table 7, the tracers' vertical zonal mean distributions
582 are shown in Figure 8, and the comparisons with the ARCTAS measurements for
583 NH_4^+ and NO_3^- are shown in Figure 9. For convenient comparison, the GMI baseline
584 results are given in the table and figures as well. There is a dramatic decrease (from 17.5
585 to 1.1 Tg) in NH_3 wet deposition when using pure water NH_3 Henry's law constant.
586 Consequently, NH_3 will remain in the atmosphere (i.e. ~ 8 times more atmospheric NH_3)
587 to produce ~1.6 times more NH_4^+ chemically. This, in turn, greatly increases atmospheric
588 NO_3^- to 0.97 Tg from 0.26 Tg reported in baseline simulation. A large portion of the
589 increased NH_3, NH_4^+ and NO_3^- resides in the upper troposphere and close to the
590 tropopause region, while the changes of the tracers in the lower troposphere are relatively
591 small, as shown in Figure 8. These accumulations at high altitudes are far above (i.e. ~ 50
592 times for NH_4^+ and NO_3^-) the ARCTAS observed tracer amounts as shown in Figure 9.
593 The TWET experiment might be an explanation of NH_4^+ and NO_3^- accumulations near the
594 tropopause region (Figure 3a-b) in the INCA model whose NH_3 Henry's law constant H^{Θ}

595 is 74 without pH correction (i.e. a L-theta model, table 5). However, it is puzzling that the
596 NH_3 simulations by GISS-MATRIX and GISS-OMA, those are the models with L-theta,
597 are closer to the simulations of the models with H-theta, i.e. no NH_4^+ and NO_3^-
598 accumulation near the tropopause and comparable removal of NH_4^+ (Figure 3a-b and
599 Table 4b).
600
601 **5.2 Contribution of dust and sea salt on nitrate formation**
602 In the presence of acidic accumulation-mode sulfuric acid containing aerosols, HNO_3,
603 NO_3 radicals, and N_2O_5 will deposit on larger alkaline mineral or salt particles (Dentener
604 et al., 1996; Gard et al., 1998; Hauglustaine 2014; Karydis et al., 2016; Murphy and
605 Thomson 1997; Paulot et al., 2016). Considerable evidence shows that the majority of
606 atmospheric nitrate is formed via reactions associated with dust and sea salt (Allen et al.
607 2015; Itahashi et al., 2016; Karydis et al., 2016). Coarse mode nitrate overwhelmingly
608 dominates over remote oceanic regions (Itahashi et al., 2016). Over wide land regions,
609 nitrate also quite often exists in the form of supermicron NO_3^- balanced by the presence
610 of mineral cations arising from transport of crustal dust and sea spray aerosol (Allen et
611 al.,2015; Lefer and Talbot; 2001).
612
613 Investigation of nitrate interactions with mineral dust and sea salt depends on the
614 simulation approach adopted in a model. The traditional equilibrium approach to partition
615 semi-volatile HNO_3 between the gas and aerosol phases is no longer possible since the
616 time to reach equilibrium on coarse mode particles (several hours to days) is typically
617 much longer than the chemical time step used in a global model (less than 1 hour) (John
618 et al., 1989; Myhre et al., 2006). Meng and Seinfeld (1996) found that on longer time
619 scales, when NH_3/HNO_3 started to condense on larger aerosols, their gas phase
620 concentrations decreased so that some of the condensed matter can be driven back to the
621 gas phase from the small semi-volatile aerosols. A fix to a non-equilibrium state would
622 be to implement a kinetic formulation for the particles that have a long equilibrium time
623 scale (Feng and Penner, 2007; Karydis et al., 2010). However, implementing explicit
624 kinetics in a global model would be computationally expensive and, hence, is not feasible
625 for long-term climate simulations. Several approximations, therefore, have been
626 developed to compromise accuracy and efficiency.
627
628 Four such approximations are adopted by the nine models participating in this study: 1)
629 using equilibrium calculations for fine mode particles only while neglecting nitrate
630 formation on coarse mode particles (CHASER and GISS-MATRIX); 2) combining
631 equilibrium calculation for a solution of SO_4^{2-}-NO_3^--NH_4^+-H_2O and heterogeneous
632 reaction calculation for nitrogen uptake on dust and sea-salt using a first-order loss rate
633 (EMEP, GMI, GISS-OMA and INCA); 3) running equilibrium model including NH_3,
634 dust and sea salt repeatedly for aerosol sizes from fine mode to coarse mode (Oslo-CTM2
635 and Oslo-CTM3); and 4) using only the fraction of the gas that can kinetically condense
636 within the time step of the model in the equilibrium calculations for each aerosol size
637 mode (EMAC).
638
639 Nitrate is formed primarily on dust and sea salt by GMI (88%) and INCA (82%) (see
640 Table 4a). INCA further separates the formation as 45% on dust and 37% on sea-salt. The

above-mentioned approach 1 is problematic due to absence of coarse mode nitrate, an important portion of nitrate, which results in relatively low nitrate burdens for CHASER and GISS-MATRIX. Unfortunately, the other models are missing a detailed nitrate chemistry budget report. A potential impact of dust and sea-salt on nitrate formation, nevertheless, can be inferred from the approach adopted by a model. For example, OsloCTM2 and OsloCTM3 adopt approach 3. Although the model allows fine mode particles to reach equilibrium first, the subsequent equilibrium calculation for coarse mode particles may still produce coarse mode nitrate too quickly, see discussion of the ratio of coarse model nitrate in the next subsection. To avoid such overestimations on the production of coarse mode nitrate, EMAC allows only a fraction of HNO_3 to partition in the aerosol phase by assuming diffusion limited condensation (Pringle et al., 2010).

To further understand the role of homogeneous and heterogeneous chemical reaction processes in nitrate formation, we conducted two more sensitivity experiments, TnoCNH3 and TnoCHET, with the GMI model (Table 6). Experiment TnoCNH3 turned off chemical conversion of NH_3 to NH_4^+ in the GMI thermodynamic equilibrium model, while experiment TnoCHET excluded the nitrate formation via heterogeneous reaction of gas HNO_3 on the particles of dust and sea salt. The budget report, vertical zonal mean distribution and model-observation comparison of NH_3, NH_4^+ and NO_3^- are given in Table 7 and Figures 8-9, respectively. It is not surprising that experiment TnoCNH3 gives a higher atmospheric NH_3 burden (0.32 Tg) compared with baseline (0.11 Tg) with little NH_4^+ left (from its initial field). The interesting thing is that the formed NO_3^- has only slightly decreased compared with baseline (from 0.26 to 0.20 Tg), confirming the importance of NO_3^- formation via dust and sea salt. For experiment TnoCHET, the simulations of NH_3 and NH_4^+ stay the same but the formed NO_3^- is decreased dramatically (from 0.26 to 0.10), indicating that NO_3^- formation via NH_3 chemistry alone in the GMI model is relatively small. The chemical production of NO_3^- is about 6 times larger in TnoCNH3 (via dust and sea salt) than in TnoCHET (via NH_3). However, the NO_3^- produced via NH_3 chemistry (TnoCHET) is non-negligible over remote regions impacted by long-range transport, as shown in the analysis of April Alaska observations in Figure 9.

5.3 Nitrate size distribution

Unlike sulfate aerosol, a noticeable fraction of nitrate aerosol is in the coarse mode. Having an accurate aerosol size distribution is critical in climate forcing estimations, since large size particles have a relatively small optical cross section at a given aerosol mass loading and the nitrate material coating on dust particles has almost no direct impact on the dust optics, although the greatly impact dust lifetime (Bauer et al., 2007). Given that the deposition velocity of a coarse particle is greater than that of a fine particle, an accurate size distribution is also necessary to estimate deposition of particulate nitrates (Yeatman et al., 2001; Sadanaga et al., 2008). This estimation is particularly important over oceans where coarse mode nitrate dominates (Itahashi et al., 2016) and nitrogen supply is often in deficit (Hansell and Follows, 2008).

As we have discussed in section 5.2, nitrate size distribution varies with the approaches adopted for nitrate formation on coarse mode aerosols (i.e. dust and sea salt). Figure 10

gives the burdens of nitrate in fine mode and coarse mode portions and the ratio between coarse mode and total (f_c) for the eight discussed models. The ratio is ranging from 0 (CHASER and GISS-OMA), ~50% (EMAC, GMI and INCA), ~80% (EMEP and OsloCTM2), and 97% (OsloCTM3). The two OsloCTMs give the highest f_c partially because they run TEQM model for coarse model particles.

A wide range of f_c, from 0 to > 90%, has been reported previously by model simulations (Adams et al., 2001; Bauer et al., 2007; Jacobson 2001), while the range is narrowed down to 40-60% for the model studies using the approach that solves dynamic mass transfer equation for coarse mode particles (Feng and Penner, 2007; Xu and Penner, 2012).

It is worth pointing out that aerosol microphysics modify aerosol size as well. For example, a process like coagulation would also allow NO_3^- to mix with other particles and enter coarse mode aerosol. New particle formation/nucleation would add $NH_3/NH_4^+/NO_3^-$ into the ultra fine mode. Except EMAC and GISS-MATRIX, majority models involved in this study are bulk aerosol models that do not account for aerosol microphysics.

It is challenging to verify the nitrate size distribution globally due to the limited measurements on time and space. Measurements over regional and station sites indicated that the ratio of f_c could be very high and vary seasonally over oceanic sites. For example, annual mean f_c during 2002-2004 from the Fukue supersite observatory is about 72% with a seasonal variation of 60–80% in winter and of around 80% in summer (Itahashi et al., 2016).

However, the ratio could be varied dramatically over land or the areas affected by land pollution. For example, observations of fine and coarse particulate nitrate at several rural locations in the United States indicated that nitrate was predominantly in submicron ammonium nitrate particles during the Bondville and San Gorgonio (April) campaigns, in coarse mode nitrate particles at Grand Canyon (May) and Great Smoky Mountains (July/August), and both fine and coarse mode nitrate during the studies at Brigantine and San Gorgonio (July) (Lee et al., 2008). Allen et al. (2015) examined aerosol composition data collected during the summer 2013 SOAS and concluded that inorganic nitrate in the southeastern United States likely exists in the form of supermicron NO_3^-, balanced by the presence of mineral cations arising from the transport of crustal dust and sea spray aerosol. The measurements over Harvard Forest, a rural site in central Massachusetts, supported that the majority of nitrate mass was associated with water-soluble supermicron soil-derived Ca^{2+} in an acidic environment (Lefer and Talbot, 2001). Measurements of coarse-mode aerosol nitrate and ammonium at two polluted coastal sites, Weybourne, England and Mace Head, Ireland, during polluted flow when the air had passed over strong source regions of the UK and northern Europe, showed 40–60% of the nitrate was found in particles with diameter >1 μm, but under clean marine conditions almost 100% conversion was seen (Yeatman et al., 2001).

6. Conclusions

We present the AeroCom phase III nitrate study by assessing aerosol simulations of nitrate and ammonium and their precursors with nine global models. Five of the models couple the chemical calculation online with meteorological simulation, and four use archived meteorological fields driving chemistry. To focus on chemical-physical processes behind the diversity of nitrate simulation, all participating models are encouraged to use HTAP2 emission inventory for aerosol and gas emissions from anthropogenic, aircraft, and ship sources. The simulated aerosols of nitrate and ammonium and their precursors are compared among the models and evaluated against various measurements including surface concentrations and dry/wet depositions from surface measurements, and vertical distributions from aircraft measurements.

All models capture the main features of the distribution of nitrate and ammonium: large surface and column amounts over China, South Asia, Europe, and U.S. These regions are typically densely populated with large NH_3 and NO_x emissions. Many models also show enhanced nitrate and ammonium over the Middle East and continents over the Southern Hemisphere. The former undergoes huge dust pollution and the latter experiences fires that emit both NH_3 and NO_x.

The diversity of nitrate and ammonium simulations among the models is large: the ratio of the maximum to minimum quantities among the nine models is 13.4 and 4.4 for model simulated global mass burdens of nitrate and ammonium, respectively, and 3.9 and 5.2 for the corresponding lifetimes. These values are also larger than those of sulfate: 4.0 for global burden and 3.0 for lifetime. The agreement between models and observations is better for aerosol components than for gas tracers. All models underestimate NH_3 surface mass concentrations but most models overestimate surface HNO_3 concentrations over North America and East Asia. Performance of NH_3 is the worst: this could partially be associated to its relatively lower measurement accuracy, i.e. a loss of ammonia possibly on the filters designed to collect NH_3 (Williams et al., 1992). Among aerosol simulations, model performance based on evaluation of surface mixing ratio and dry/wet depositions is very similar for NH_4^+ and SO_4^{2-}, while slightly worse for NO_3^-. Models severely underestimate the aerosol concentrations with only a few exceptions when compared with aircraft measurements and this problem is worse over regions impacted by long-range transport than those closer to sources.

There are many intrinsic reasons for a larger diversity in nitrate simulations among models. Nitrate is involved in much more complicated chemistry: the chemical mechanism needs to handle a multiphase multicomponent solution system. The system sometimes cannot even be solved using the thermodynamic equilibrium approach when coarse mode dust and sea salt particles present. A reasonable nitrate simulation also depends on good simulations of various precursors, such as NH_3, HNO_3, dust and sea salt, although models account for impact of dust and sea salt very differently. Even an accurate simulation of SO_4^{2-} is a prerequisite because SO_4^{2-} surpasses NO_3^- at reacting with NH_4^+.

The models' intercomparison and model-observation comparison revealed at least two critical issues in nitrate simulation that demand further exploration: NH_3 wet deposition

and relative contribution to NO_3^- formation via NH_3 and dust/sea salt. The nine participating models adopt very different effective Henry's law constants for NH_3, with one group having a value equal or less than 100 (in pure water) and the other larger than 1.e+05 (with pH correction). Sensitivity studies using the GMI model indicated that without pH correction, NH_3 wet deposition decreases massively (from 17.5 to 1.1 Tg), which prolongs atmospheric NH_3 lifetime (from 0.67 to 5.2 days) and enhances its atmospheric burden (from 0.11 to 0.85 Tg), and thus the atmospheric burden of NH_4^+ (from 0.17 to 0.48 Tg) and NO_3^- (from 0.26 to 0.97 Tg) as well. These enhanced tracers tend to accumulate in the upper troposphere and close to the tropopause, and are too high when compared with aircraft measurements. Since liquid-phase reaction 2 in Appendix can reach equilibrium quickly within a chemical time step, we recommend including it in accounting for NH3 solution. Theoretically, a more accurate approach is to combine wet removal with liquid-phase chemistry calculation. In other words, instead of using an implicit calculation of effective Henry's law constant, the gas-liquid phase equilibrium is explicitly calculated based on the chemical mechanism used in the liquid phase. The solution of NH_3 is calculated by solving a set of partial differential equations, which includes not only the gas-liquid phase equilibrium, but also all the important reactions in the liquid phase, as adopted in EMAC model.

All the models use thermodynamic equilibrium to solve the chemical process of NH_3/NH_4^+ to NO_3^- formation in fine mode aerosols. However, the models adopt very different ways in accounting for the contribution of these reactions on the surface of dust and sea salt particles: some account for both dust and sea salt, some account for only dust or only sea salt, and two models even do not account for any heterogeneous reactions. The methodologies that take dust and sea salt into account are also very different, i.e. together with NH_4^+ using thermodynamic equilibrium model or simply adopting a first order loss rate on dust and sea salt surfaces. The chemical budget reported by GMI and INCA indicates that the majority (>80%) of global NO_3^- formation is via reaction on dust and sea salt. Two sensitivity experiments using the GMI model by tagging the NO_3^- formation from either NH_3/NH_4^+ chemistry or heterogeneous reactions on dust and sea salt confirm the critical importance of the latter process, and indicate that the former process is relatively important in remote regions. The importance of NO_3^- formation on dust and sea salt lies also in its determination on nitrate particle size distribution, so that has an implication in air quality and climate studies as well.

Our work presents a first effort to assess nitrate simulation from chemical and physical processes. A companion study is proposed by AeroCom III nitrate activity to investigate how sensitive is nitrate formation in response to the possible future changes of emission and meteorological fields. These perturbation fields include increasing NH_3 emission, decreasing NOx, SOx and dust emissions, and increasing atmospheric temperature and relative humidity. It would be particularly interesting to examine how aerosol pH changes and its influence on atmospheric acid/base gas-particle system during the experiment. Future aerosol pH does not necessarily increase with SO_2 emission reduction. Indeed, studies over US southeast indicated that its aerosol has been getting more acidic over the past decade although SO_2 emission decreased and NH_3 emission stayed constant [Silvern et al., 2017; Weber et al., 2016]. This environment of high aerosol acidity hinders the

formation of nitrate aerosol, which only occurs when pH is over ~2 to 3 [Weber et al., 2016]. In addition, understanding why and how the system is insensitive to changing SO_2 level due to buffering of the partitioning of semivolatile NH_3 over regions such as US southeast helps us to gain some insight into how errors in sulfate (and ammonium) may propagate to errors in aerosol nitrate. In particular, the correlation between model predictions and observations for SO_4^{2-} and NH_4^+ is quite poor for some models (Figure 4). It would be also interesting to include organic gas/aerosol into the system since they are not only important atmospheric components, but also reduce the uptake of NH_3. Competition for uptake between NH_3 and organic gases considerably slows down the approach to thermodynamic equilibrium [Silvern et al., 2017]. Based on the findings of this work, modelers should pay particular attention to incorporating dust and sea salt and treating NH_3 wet deposition to improve nitrate simulation. Further evaluation using satellite measurements, such as NH_3 products from IASI and TES, is desired and will be conducted. Such evaluation requires global 3-dimensional high frequency model data. Potential future study also includes estimation of nitrate forcing for climate change.

Appendix

For some acidic/basic gases, including NH_3, Henry's law constant is also a function of pH in water (a.k.a effective Henry's law constant). This is because not only does the aqueous chemistry reaction $NH_3 + H_2O$ (equation 1) reach equilibrium within a chemical time step but its product $NH_3 \cdot H_2O$ (equation 2) does as well.

$$NH_3 + H_2O \Leftrightarrow NH_3 \cdot H_2O \quad (1)$$

$$NH_3 \cdot H_2O \Leftrightarrow NH_4^+ + OH^- \quad (2)$$

Here, NH_4^+ is the ammonium ion and OH^- is the hydroxide ion. The total dissolved ammonia $[NH_3^T]$ is given by

$$\begin{aligned}[NH_3^T] &= [NH_3 \cdot H_2O] + [NH_4^+] \\ &= p_{NH3} H^\Theta \left(1 + \frac{K_{al}[\mathrm{H}^+]}{K_w}\right) \\ &\approx p_{NH3} \left(H^\Theta \frac{K_{al}[H^+]}{K_w}\right) \quad (3)\end{aligned}$$

Here, p_{NH3} is the partial pressure of NH_3, $K_{al} = [NH_4^+][OH^-] / [NH_3 \bullet H_2O] \approx 1.8 \times 10^{-5}$, and $K_w = 1.0 \times 10^{-14}$ at 298 K in pure water. So the effective Henry's law constant $H^{\Theta *}$ is inferred from H^Θ with a correction of pH ($pH = -\log_{10}[H^+]$) as

$$H^{\Theta *} = H^\Theta \frac{K_{al}[H^+]}{K_w} \quad (4)$$

References:

Allen1,H. M., D. C. Draper1, B. R. Ayres, A. Ault, A. Bondy, S. Takahama, R. L. Modini, K. Baumann, E. Edgerton, C. Knote, A. Laskin, B. Wang, and J. L. Fry, Influence of crustal dust and sea spray supermicron particle concentrations and acidity on inorganic NO3 aerosol during the 2013 Southern Oxidant and Aerosol Study, Atmos. Chem. Phys., 15, 10669–10685, 2015, www.atmos-chem-phys.net/15/10669/2015/, doi:10.5194/acp-15-10669-2015.

Bauer, S. E., Balkanski, Y., Schulz, M., Hauglustaine, D. A., and Dentener, F.: Global modeling of heterogeneous chemistry on mineral aerosol surfaces: Influence on tropospheric ozone chemistry and comparison to observations, J. Geophys. Res.-Atmos., 109, D02304, doi:10.1029/2003jd003868, 2004.

Bauer, S.E., and D. Koch, 2005: Impact of heterogeneous sulfate formation at mineral dust surfaces on aerosol loads and radiative forcing in the Goddard Institute for Space Studies general circulation model. J. Geophys. Res., 110, D17202, doi:10.1029/2005JD005870.

Bauer, S. E., Koch, D., Unger, N., Metzger, S. M., Shindell, D. T., and Streets, D. G.: Nitrate aerosols today and in 2030: a global simulation including aerosols and tropospheric ozone, Atmos. Chem. Phys., 7, 5043–5059, doi:10.5194/acp-7-5043-2007, 2007.

Bauer, S.E., D. Wright, D. Koch, E.R. Lewis, R. McGraw, L.-S. Chang, S.E. Schwartz, and R. Ruedy, 2008: MATRIX (Multiconfiguration Aerosol TRacker of mIXing state): An aerosol microphysical module for global atmospheric models. Atmos. Chem. Phys., 8, 6603-6035, doi:10.5194/acp-8-6003-2008.

Bauer, S. E., K. Tsigaridis, and R. Miller, Significant atmospheric aerosol pollu4on caused by world food cultivation, Geophys. Res. Lett., 43, no. 10, 5394-5400, doi:10.1002/2016GL068354, 2016.

Bessagnet, B. and Rouïl, L.: Feedback on and analysis of the PM pollution episode in March 2014, presentation at 19-th EIONET Workshop on Air Quality Assessment and Management Berne, Switzerland, 30 September and 1 October 2014, 2014.

Bey, I, D.J. Jacob, R.M. Yantosca, J.A. Logan, B.D. Field, A.M. Fiore, Q. Li, H.Y. Liu, L.J. Mickley, M.G. Schultz, 2001: Global modeling of tropospheric chemistry with assimilated meteorology: Model description and evaluation. J. Geophys. Res., 106, 23073-23078 (2001JD000807.

Bellouin, N., Rae, J., Jones, A., Johnson, C., Haywood, J., and Boucher, O.: Aerosol forcing in the Climate Model Intercomparison Project (CMIP5) simulations by HadGEM2-ES and the role of ammonium nitrate, J. Geophys. Res.-Atmos., 116, D20206, doi:10.1029/2011jd016074, 2011.

Berntsen, T. K. and Isaksen, I. S. A.: A global three-dimensional chemical transport model for the troposphere.1. Model description and CO and ozone results, J. Geophys. Res.-Atmos., 102(D17), 21 239–21 280, 1997.

Bian, H., and C. S. Zender (2003), Mineral dust and global tropospheric chemistry: The relative roles of photolysis and heterogeneous uptake. J. Geophys. Res., 108, 4672.

Bian, H., Chin, M., Rodriguez, J. M., Yu, H., Penner, J. E., and Strahan, S., 2009: Sensitivity of aerosol optical thickness and aerosol direct radiative effect to relative humidity, Atmos. Chem. Phys., 9, 2375-2386, doi:10.5194/acp-9-2375-2009.

Bian, H., Colarco, P. R., Chin, M., Chen, G., Rodriguez, J. M., Liang, Q., Blake, D., Chu, D. A., da Silva, A., Darmenov, A. S., Diskin, G., Fuelberg, H. E., Huey, G., Kondo, Y., Nielsen, J. E., Pan, X., and Wisthaler, A.: Source attributions of pollution to the Western Arctic during the NASA ARCTAS field campaign, Atmos. Chem. Phys., 13, 4707-4721, doi:10.5194/acp-13-4707-2013, 2013.

Bouwman, A.F., Lee, D.S., Asman, W.A.H., Dentener, F.J., Van Der Hoek, K.W. and J.G.J. Olivier (1997). A Global High-Resolution Emission Inventory for Ammonia, Global Biogeochemical Cycles, 11:4, 561-587. http://www.rivm.nl/.

Chin, M., P. Ginoux, S. Kinne, B. N. Holben, B. N. Duncan, R. V. Martin, J. A. Logan, A. Higurashi, and T. Nakajima, 2002: Tropospheric aerosol optical thickness from the GOCART model and comparisons with satellite and sun photometer measurements, J. Atmos. Sci. 59, 461-483.

Cubison, M.J., A.M. Ortega, P.L. Hayes, D.K. Farmer, D.Day, M.J. Lechner, W.H. Brune, E. Apel, G.S. Diskin, J.A. Fisher, H.E. Fuelberg, A. Hecobian, D.J. Knapp, T. Mikoviny, D. Riemer, G.W. Sachse, W. Sessions, R.J. Weber, A.J. Weinheimer, A. Wisthaler, and J.L. Jimenez (2011), Effects of Aging on Organic Aerosol from Open Biomass Burning Smoke in Aircraft & Lab Studies. Atmos. Chem. and Phys. Disc. 11, 12103-12140, doi:10.5194/acpd-11-12103-2011.

DeCarlo, P. F., Kimmel, J. R., Trimborn, A., Northway, M. J., Jayne, J. T., Aiken, A. C., Gonin, M., Fuhrer, K., Horvath, T., Docherty, K. S., Worsnop, D. R., and Jimenez, J. L.: Field-deployable, high-resolution, time-of-flight aerosol mass spectrometer, Anal. Chem., 78(24), 8281–8289, 2006.

Dentener, F. J., G. R. Carmichael, Y. Zhang, J. Lelieveld, and P. J. Crutzen, Role of mineral aerosol as a reactive surface in the global troposphere, J. Geophys. Res, 101, 22,869-22889, 1996.

Dentener, F., Kinne, S., Bond, T., Boucher, O., Cofala, J., Generoso, S., Ginoux, P., Gong, S., Hoelzemann, J. J., Ito, A., Marelli, L., Penner, J. E., Putaud, J.-P., Textor, C., Schulz, M., van der Werf, G. R., and Wilson, J.: Emissions of primary aerosol and precursor gases in the years 2000 and 1750 prescribed data-sets for AeroCom, Atmos. Chem. Phys., 6, 4321–4344, doi:10.5194/acp-6-4321-2006, 2006.

Ensberg, J. J., Craven, J. S., Metcalf, A. R., Allan, J. D., Angevine, W. M., Bahreini, R., Brioude, J., Cai, C., Coe, H., de Gouw, J. A., Ellis, R. A., Flynn, J. H., Haman, C. L., Hayes, P. L., Jimenez, J. L., Lefer, B. L., Middlebrook, A. M., Murphy, J. G., Neuman, J. A., Nowak, J. B., Roberts, J. M., Stutz, J.,

Taylor, J. W., Veres, P. R., Walker, J. M., and Seinfeld, J. H.: Inorganic and black carbon aerosols in the Los Angeles Basin during CalNex, Journal of Geophysical Research-Atmospheres, 118, 1777-1803, 2013.

Fairlie, T. D., Jacob, D. J., Dibb, J. E., Alexander, B., Avery, M. A., van Donkelaar, A., and Zhang, L.: Impact of mineral dust onnitrate, sulfate, and ozone in transpacific Asian pollution plumes, Atmos. Chem. Phys., 10, 3999–4012, doi:10.5194/acp-10-3999- 2010, 2010.

Feng, Y. and Penner, J. E.: Global modeling of nitrate and ammonium: Interaction of aerosols and tropospheric chemistry, J. Geophys. Res.-Atmos., 112, D01304, doi:10.1029/2005jd006404, 2007.

Fenn, M. E., M. A. Poth, D. W. Johnson, Evidence for nitrogen saturation in the San Bernardino Mountains in southern California, Forest Ecology and Management , Volume 82, Issues 1–3, April 1996, Pages 211-230.

Fitzgerald, J. W. (1975), Approximation formulas for equilibrium size or an aerosol particle as a function of its dry size and composition and ambient relative humidity, J. Appl. Meteorol., 14(6), 1044-1049.

Fowler, Z. K., M. B. Adams, W. T. Peterjohn,Will more nitrogen enhance carbon storage in young forest stands in central Appalachia? Forest Ecology and Management, Volume 337, Pages 144–152, 1 February 2015.

Galloway, J. N., Dentener, F. J., Capone, D. G., Boyer, E. W., Howarth, R. W., Seitzinger, S. P., Asner, G. P., Cleveland, C. C., Green, P. A., Holland, E. A., Karl, D. M., Michaels, A. F., Porter, J. H., Townsend, A. R. and Vorosmarty, C. J.: Nitrogen cycles: Past, present, and future, Biogeochemistry, 70, 153–226, 2004.

Ginoux, P., M. Chin, I. Tegen, J. Prospero, B. Holben, O. Dubovik, and S.-J. Lin, 2001: Sources and global distributions of dust aerosols simulated with the GOCART model, J. Geophys. Res., 106, 20,255-20,273.

Grieshop, A. P., Robinson, A. L., Duplissy, J., Smith, J. D., Wilson, K. R., Lanz, V. A., Hueglin, C., Sun, Y. L., Tian, J., Laaksonen, A., Raatikainen, T., Rautiainen, J., Vaattovaara, P., Ehn, M., Kulmala, M., Tomlinson, J. M., Collins, D. R., Cubison, M. J., Dunlea, E. J., Huffman, J. A., Onasch, T. B., Alfarra, M. R., Williams, P. I., Bower, K., Kondo, Y., Schneider, J., Drewnick, F., Borrmann, S., Weimer, 5 S., Demerjian, K., Salcedo, D., Cottrell, L., Griffin, R., Takami, A., Miyoshi, T., Hatakeyama, S., Shimono, A., Sun, J. Y., Zhang, Y. M., Dzepina, K., Kimmel, J. R., Sueper, D., Jayne, J. T., Herndon, S. C., Trimborn, A. M., Williams, L. R., Wood, E. C., Middlebrook, A. M., Kolb, C. E., Baltensperger, U., and Worsnop, D. R.: Evolution of organic aerosols in the atmosphere, Science, 326, 1525–1529, 2009.

Hansell, D.A., Follows, M.J., 2008. Nitrogen in the Atlantic Ocean. In: Mullholland, M., Bronk, D., Capone, D., Carpenter, E. (Eds.), Nitrogen in the Marine Environment, second ed. Academic Press, pp. 597–630.

Hauglustaine, D. A., Hourdin, F., Walters, S., Jourdain, L., Filiberti, M.-A., Larmarque, J.-F., and Holland, E. A.: Interactive chemistry in the Laboratoire de Météorologie Dynamique general circulation model: description and background tropospheric chemistry evaluation, J. Geophys. Res., 109, D04314, doi:10.1029/2003JD003957, 2004.

Hauglustaine, D. A., Balkanski, Y., and Schulz, M.: A global model simulation of present and future nitrate aerosols and their direct radiative forcing of climate, Atmos. Chem. Phys., 14, 11031–11063, doi:10.5194/acp-14-11031-2014, 2014.

Haywood, J., Bush, M., Abel, S., Claxton, B., Coe, H., Crosier, J., Harrison, M., Macpherson, B., Naylor, M., and Osborne, S.: Prediction of visibility and aerosol within the operational Met Office Unified Model II?: Validation of model performance using observational data, Q. J. Roy. Meteorol. Soc., 134, 1817–1832, doi:10.1002/qj.275, 2008.

Heald, C. L., Collett Jr., J. L., Lee, T., Benedict, K. B., Schwandner, F. M., Li, Y., Clarisse, L., Hurtmans, D. R., Van Damme, M., Clerbaux, C., Coheur, P.-F., Philip, S., Martin, R. V., and Pye, H. O. T.: Atmospheric ammonia and particulate inorganic nitrogen over the United States, Atmos. Chem. Phys., 12, 10295–10312, doi:10.5194/acp-12-10295-2012, 2012.

Hess, M., P. Koepke and I. Schult, Optical properties of aerosols and clouds: The software package OPAC. Bull. Amer. Meteorol. Soc., 79(5): 831-844, 1998.

Huffman, J. A., J. T. Jayne, F. Drewnick, A. C. Aiken, T. Onasch, D. R. Worsnop, and J. L. Jimenez, Design, Modeling, Optimization, and Experimental Tests of a Particle Beam Width Probe for the Aerodyne Aerosol Mass Spectrometer, Aerosol Sci Technol. 39, 1143-1163, 2005.

Huneeus, N., M. Schulz, Y. Balkanski, J. Griesfeller, S. Kinne, J. Prospero, S. Bauer, O. Boucher, M. Chin, F. Dentener, T. Diehl, R. Easter, D. Fillmore, S. Ghan, P. Ginoux, A. Grini, L. Horowitz, D. Koch, M.C. Krol, W. Landing, X. Liu, N. Mahowald, R.L. Miller, J.-J. Morcrette, G. Myhre, J.E. Penner, J.P. Perlwitz, P. Stier, T. Takemura, and C. Zender, 2011: Global dust model intercomparison in AeroCom phase I. *Atmos. Chem. Phys.*, 11, 7781-7816, doi:10.5194/acp-11-7781-2011.

IPCC: (Intergovernmental Panel on Climate Change): The physical science basis. Contribution of working group I to the fifth assessment report of the intergovernmental panel on climate change. T.F. Stocker, D. Qin, G.-K. Plattner, M. Tignor, S.K. Allen, J. Boschung, A. Nauels, Y. Xia, V. Bex, and P.M. Midgley (eds.). Cambridge University Press, Cambridge, United Kingdom and New York, NY, USA, 2013. 2013.

Jimenez, J. L., Canagaratna, M. R., Donahue, N. M., Prevot, A. S. H., Zhang, Q., Kroll, J. H., DeCarlo, P. F., Allan, J. D., Coe, H., Ng, N. L., Aiken, A. C., Docherty, K. S., Ulbrich, I. M.,

Jacob, D. J., Crawford, J. H., Maring, H., Clarke, A. D., Dibb, J. E., Emmons, L. K., Ferrare, R. A., Hostetler, C. A., Russell, P. B., Singh, H. B., Thompson, A. M., Shaw, G. E., McCauley, E., Pederson, J. R., and Fisher, J. A.: The Arctic Research of the Composition of the Troposphere from Aircraft and Satellites (ARCTAS) mission: design, execution, and first results, Atmos. Chem. Phys., 10, 5191–5212, doi:10.5194/acp-10-5191-2010, 2010.

Janssens-Maenhout, G., Crippa, M., Guizzardi, D., Dentener, F., Muntean, M., Pouliot, G., Keating, T., Zhang, Q., Kurokawa, J., Wankmüller, R., Denier van der Gon, H., Kuenen, J. J. P., Klimont, Z., Frost, G., Darras, S., Koffi, B., and Li, M.: HTAP_v2.2: a mosaic of regional and global emission grid maps for 2008 and 2010 to study hemispheric transport of air pollution, Atmos. Chem. Phys., 15, 11411-11432, doi:10.5194/acp-15-11411-2015, 2015

Jöckel, P., Kerkweg, A., Pozzer, A., Sander, R., Tost, H., Riede, H., Baumgaertner, A., Gromov, S., and Kern, B.: Development cycle 2 of the Modular Earth Submodel System (MESSy2), Geosci. Model Dev., 3, 717–752, doi:10.5194/gmd-3-717-2010, 2010.

John,W., S. M.Wall, J. L. Ondo, and W. Winklmayr (1989), Acidic-aerosol size distributions during SCAQS (Southern California Air Quality Study), final report, Rep. CA/DOH/AIHL/SP-51, Calif. Air Resour. Board, Sacramento.

Kanakidou, M., R.A. Duce, J.M. Prospero, A.R. Baker, C. Benitez-Nelson, F.J. Dentener, K.A. Hunter, P.S. Liss, N. Mahowald, G.S. Okin, M. Sarin, K. Tsigaridis, M. Uematsu, L.M. Zamora, and T. Zhu, 2012: Atmospheric fluxes of organic N and P to the global ocean. Glob. Biogeochem. Cycles, 26, GB3026, doi:10.1029/2011GB004277.

Kanakidou, M., S. Myriokefalitakis, N. Daskalakis, G. Fanourgakis, A. Nenes, A. Baker, K. Tsigaridis, and N. Mihalopoulos, 2016: Past, present and future atmospheric nitrogen deposition. J. Atmos. Sci., 73, no. 5, 2039-2047, doi:10.1175/JAS-D-15-0278.1.

Karydis, V. A., Tsimpidi, A. P., Fountoukis, C., Nenes, A., Zavala, M., Lei, W., Molina, L. T., and Pandis, S. N.: Simulating the fine and coarse inorganic particulate matter concentrations in a polluted megacity, Atmospheric Environment, 44, 608-620, 2010.

Karydis, V. A., Tsimpidi, A. P., Lei, W., Molina, L. T., and Pandis, S. N.: Formation of semivolatile inorganic aerosols in the Mexico City Metropolitan Area during the MILAGRO campaign, Atmospheric Chemistry and Physics, 11, 13305-13323, 2011.

Karydis, V. A., A. P. Tsimpidi, A. Pozzer, M. Astitha, and J. Lelieveld, 2016: Effects of mineral dust on global atmospheric nitrate concentrations. Atmos. Chem. Phys., 16, 1491–1509, doi:10.5194/acp-16-1491-2016.

Kim, Y. P., Seinfeld, J. H., and Saxena, P.: Atmospheric gas–aerosol equilibrium I. Thermodynamic model, Aerosol Sci. Technol., 19, 157–181, 1993.

Kim, D., M. Chin, H. Yu, T. Diehl, Q. Tan, R.A. Kahn, K. Tsigaridis, S.E. Bauer, T. Takemura, L. Pozzoli, N. Bellouin, M. Schulz, S. Peyridieu, A. Chédin, and B. Koffi, 2014: Sources, sinks, and transatlantic transport of North African dust aerosol: A multi-model analysis and comparison with remote-sensing data. *J. Geophys. Res. Atmos.*, 119, no. 10, 6259-6277, doi:10.1002/2013JD021099.

Kinne, S., Schulz, M., Textor, C., Guibert, S., Balkanski, Y., Bauer, S. E., Berntsen, T., Berglen, T. F., Boucher, O., Chin, M., Collins, W., Dentener, F., Diehl, T., Easter, R., Feichter, J., Fillmore, D., Ghan, S., Ginoux, P., Gong, S., Grini, A., Hendricks, J., Herzog, M., Horowitz, L., Isaksen, I., Iversen, T., Kirkevåg, A., Kloster, S., Koch, D., Kristjansson, J. E., Krol, M., Lauer, A., Lamarque, J. F., Lesins, G., Liu, X., Lohmann, U., Montanaro, V., Myhre, G., Penner, J., Pitari, G., Reddy, S., Seland, O., Stier, P., Takemura, T., and Tie, X.: An AeroCom initial assessment – optical properties in aerosol

component modules of global models, Atmos. Chem. Phys., 6, 1815–1834, doi:10.5194/acp-6-1815-2006, 2006.
Koch, D., M. Schulz, S. Kinne, C. McNaughton, J.R. Spackman, T.C. Bond, Y. Balkanski, S. Bauer, T. Berntsen, O. Boucher, M. Chin, A. Clarke, N. De Luca, F. Dentener, T. Diehl, O. Dubovik, R. Easter, D.W. Fahey, J. Feichter, D. Fillmore, S. Freitag, S. Ghan, P. Ginoux, S. Gong, L. Horowitz, T. Iversen, A. Kirkevåg, Z. Klimont, Y. Kondo, M. Krol, X. Liu, R.L. Miller, V. Montanaro, N. Moteki, G. Myhre, J.E. Penner, J.P. Perlwitz, G. Pitari, S. Reddy, L. Sahu, H. Sakamoto, G. Schuster, J.P. Schwarz, Ø. Seland, P. Stier, N. Takegawa, T. Takemura, C. Textor, J.A. van Aardenne, and Y. Zhao, 2009: Evaluation of black carbon estimations in global aerosol models. *Atmos. Chem. Phys.*, 9, 9001-9026, doi:10.5194/acp-9-9001-2009.
Kinnison, D. E., P. S. Connell, J. Rodriguez, D. B. Considine, D. A. Rotman, J. Tannahill, R. Ramaroson, A. Douglass, S. Baughcum, L. Coy, P. Rasch, D. Waugh, 2001: The Global Modeling Initiative assessment model: Application to high-speed civil transport perturbation, J. Geophys. Res., 106, 1693-1712.
Lacis, A. A., Refractive Indices of Three Hygroscopic Aerosols and their Dependence on Relative Humidity, http://gacp.giss.nasa.gov/data_sets/lacis/introduction.pdf.
Lamarque, J.-F., J. T. Kiehl, G. P. Brasseur, T. Butler, P. Cameron-Smith, et al. (2005), Assessing future nitrogen deposition and carbon cycle feedback using a multimodel approach : Analysis of nitrogen deposition, J. of Geophys. Res., Vol. 110, D19303, doi: 10.1029/2005JD005825.
Lee, T., X.-Y. Yu, B. Ayres, S. M. Kreidenweis, W. C. Malm, J. L. Collett Jr., Observations of fine and coarse particle nitrate at several rural locations in the United States, Atmospheric Environment 42, 2720–2732, 2008.
Li, J., W.-C. Wang, H. Liao, and W. Chang. 2014. Past and future direct radiative forcing of nitrate aerosol in East Asia. Theor. Appl. Climatol. 1–14. doi:10.1007/s00704-014-1249-1.
Liao, H., P. J. Adams, S. H. Chung, J. H. Seinfeld, L. J. Mickley, and D. J. Jacob (2003), Interactions between tropospheric chemistry and aerosols in a unified general circulation model, J. Geophys. Res., 108(D1), 4001, doi:10.1029/2001JD001260.
Liu, X., J. E. Penner, S. J. Ghan, and M. Wang, 2007: Inclusion of Ice Microphysics in the NCAR Community Atmospheric Model Version 3 (CAM3). J. Climate, 20, 4526-4547.
Liu, Y., G. Gibson, C. Cain, H. Wang, G. Grassian, and A. Laskin (2008) Kinetics of Heterogeneous Reaction of CaCO3Particles with Gaseous HNO3 over a Wide Range of Humidity, J. Physical Chemistry A, doi:10.1021/jp076169h
Malm, W. C., Schichtel, B. A., Pitchford, M. L., Ashbaugh, L. L., and Eldred, R. A.: Spatial and monthly trends in speciated fine particle concentration in the United States, J. Geophys. Res. Atmos., 109(D3), D03306, doi:10.1029/2003/JD003739, 2004.
Metzger, S., F. Dentener, S. Pandis, and J. Lelieveld (2002), Gas/aerosol partitioning: 1. A computationally efficient model, J. of Geophys. Res. Vol. 107, No. D16, 4312, 10.1029/2001JD001102.
Mezuman, K., S.E. Bauer, and K. Tsigaridis, 2016: Evaluating secondary inorganic aerosols in three dimensions. Atmos. Chem. Phys., 16, 10651-10669, doi:10.5194/acp-16-10651-2016.
Milegroet, H. Van and D. W. Cole, The Impact of Nitrification on Soil Acidification and Cation Leaching in a Red Alder Ecosystem, ACSESS, Alliance of Crop, Soil, and Environmental Science Societies, doi:10.2134/jeq1984.00472425001300040015x ,1984
Myhre, G., A. Grini, and S. Metzger (2006), Modeling of nitrate and ammonium-containing aerosols inpresence of sea salt, Atmos. Chem. Phys., 6, 4809-4821, www.atmos-chem-phys.net/6/4809/2006/.
Myhre, G., B. H., Samset, M. Schulz, Y. Balkanski, S. Bauer, T. K. Berntsen, H. Bian, N. Bellouin, M. Chin, T. Diehl, R. C. Easter, J. Feichter, S. J. Ghan, D. Hauglustaine, T. Iversen, S. Kinne, A. Kirkevåg, J.-F. Lamarque, G. Lin, X. Liu, G. Luo, X. Ma, J. E. Penner, P. J. Rasch, Ø. Seland, R. B. Skeie, P. Stier, T. Takemura, K. Tsigaridis, Z. Wang, L. Xu, H. Yu, F. Yu, J.-H. Yoon, K. Zhang, H. Zhang, and C. Zhou, Radiative forcing of the direct aerosol effect from AeroCom Phase II simulations, Atmos. Chem. Phys., 13, 1853-1877, doi:10.5194/acp-13-1853-2013, 2013.
Nowak, J., J. B., Weinheimer, A. J., Hoff, R. M., Berkoff, T. A., Beyersdorf, A. J., Olson, J., Crawford, J. H., and Cohen, R. C.: On the effectiveness of nitrogen oxide reductions as a control over ammonium nitrate aerosol, Atmos. Chem. Phys., 16, 2575–2596, doi:10.5194/acp-16-2575-2016, 2016
Paulot, F., Ginoux, P., Cooke, W. F., Donner, L. J., Fan, S., Lin, M.-Y., Mao, J., Naik, V., and Horowitz, L. W.: Sensitivity of nitrate aerosols to ammonia emissions and to nitrate chemistry: implications for

present and future nitrate optical depth, Atmos. Chem. Phys., 16, 1459–1477, doi:10.5194/acp-16-1459-2016, http://www.atmos-chem-phys.net/16/1459/2016/, 2016.

Phoenix, G., W. K. Hicks, S. Cinderby, J. C. I. Kuylenstierna, W. D. Stock, et al. (2006), Atmospheric nitrogen deposition in world biodiversity hotspots: the need for a greater global perspective in assessing N deposition impacts, Global Change Biology, 12, 470-476, doi: 10.1111/j.1365-2486.2006.01104.x.

Prentice, M. J., et al. (2001), The carbon cycle and atmospheric carbon dioxide, in Climate Change 2001, pp. 184-237, Cambridge Univ. Press, New York.

Pringle, K. J., Tost, H., Message, S., Steil, B., Giannadaki, D., Nenes, A., Fountoukis, C., Stier, P., Vignati, E., and Leieved, J.: Description and evaluation of GMXe: a new aerosol submodel for global simulations (v1), Geoscientific Model Development, 3, 391-412, 2010.

Pusede, S. E., Duffey, K. C., Shusterman, A. A., Saleh, A., Laughner, J. L., Wooldridge, P. J., Zhang, Q., Parworth, C. L., Kim, H., Capps, S. L., Valin, L. C., Cappa, C. D., Fried, A., Walega, Riemer, N., H. Vogel, B. Vogel, B. Schell, I. Ackermann, C. Kessler, and H. Hass (2003), Impact of the heterogeneous hydrolysis of N2O5 on chemistry and nitrate aerosol formation in the lower troposphere under photosmog conditions, J. Geophys. Res., 108(D4), 4144, doi:10.1029/2002JD002436.

Sander, S. P., J. Abbatt, J. R. Barker, J. B. Burkholder, R. R. Friedl, D. M. Golden, R. E. Huie, C. E. Kolb, M. J. Kurylo, G. K. Moortgat, V. L. Orkin and P. H. Wine "Chemical Kinetics and Photochemical Data for Use in Atmospheric Studies, Evaluation No. 17," JPL Publication 10-6, Jet Propulsion Laboratory, Pasadena, 2011 http://jpldataeval.jpl.nasa.gov.

Saxena, P., Hudischeyskyj, A. B., Seigneur, C., and Seinfeld, J. H., A comparative study of equilibrium approaches to the chemical characterization of secondary aerosols, Atmos. Enuiron. 20:1471- 1483, 1986.

Schaap, M., Müller, K., & Ten Brink, H. M. (2002). Constructing the European aerosol nitrate concentration field from quality analysed data. Atmospheric Environment, 36(8), 1323-1335.

Schaap, M., van Loon, M., ten Brink, H. M., Dentener, F. J., and Builtjes, P. J. H.: Secondary inorganic aerosol simulations for Europe with special attention to nitrate, Atmos. Chem. Phys., 4, 857-874, doi:10.5194/acp-4-857-2004, 2004.

Schmidt, G.A., M. Kelley, L. Nazarenko, R. Ruedy, G.L. Russell, I. Aleinov, M. Bauer, S.E. Bauer, M.K. Bhat, R. Bleck, V. Canuto, Y.-H. Chen, Y. Cheng, T.L. Clune, A. Del Genio, R. de Fainchtein, G. Faluvegi, J.E. Hansen, R.J. Healy, N.Y. Kiang, D. Koch, A.A. Lacis, A.N. LeGrande, J. Lerner, K.K. Lo, E.E. Matthews, S. Menon, R.L. Miller, V. Oinas, A.O. Oloso, J.P. Perlwitz, M.J. Puma, W.M. Putman, D. Rind, A. Romanou, M. Sato, D.T. Shindell, S. Sun, R.A. Syed, N. Tausnev, K. Tsigaridis, N. Unger, A. Voulgarakis, M.-S. Yao, and J. Zhang, 2014: Configuration and assessment of the GISS ModelE2 contributions to the CMIP5 archive. J. Adv. Model. Earth Syst., 6, no. 1, 141-184, doi:10.1002/2013MS000265.

Schulz, M., Textor, C., Kinne, S., Balkanski, Y., Bauer, S., Berntsen, T., Berglen, T., Boucher, O., Dentener, F., Guibert, S., Isaksen, I. S. A., Iversen, T., Koch, D., Kirkevåg, A., Liu, X., Montanaro, V., Myhre, G., Penner, J. E., Pitari, G., Reddy, S., Seland, Ø., Stier, P., and Takemura, T.: Radiative forcing by aerosols as derived from the AeroCom present-day and pre-industrial simulations,Atmos. Chem. Phys., 6, 5225–5246, doi:10.5194/acp-6-5225-2006, 2006.

Schutgens, N. A. J., Gryspeerdt, E., Weigum, N., Tsyro, S., Goto, D., Schulz, M. and Stier, P.: Will a perfect model agree with perfect observations? The impact of spatial sampling, Atmos. Chem. Phys., 16(10), 6335-6353, 2016.

Shindell, D. T., Faluvegi, G., and Bell, N.: Preindustrial-to-present-day radiative forcing by tropospheric ozone from improved simulations with the GISS chemistry-climate GCM, Atmos. Chem. Phys., 3, 1675–1702, 2003.

Silvern, R. F., Jacob, D. J., Kim, P. S., Marais, E. A., Turner, J. R., Campuzano-Jost, P., and Jimenez, J. L.: Inconsistency of ammonium–sulfate aerosol ratios with thermodynamic models in the eastern US: a possible role of organic aerosol, Atmos. Chem. Phys., 17, 5107-5118, 10.5194/acp-17-5107-2017, 2017.

Simpson, D., Benedictow, A., Berge, H., Bergström, R., Emberson, L. D., Fagerli, H., Flechard, C. R., Hayman, G. D., Gauss, M., Jonson, J. E., Jenkin, M. E., Nyíri, A., Richter, C., Semeena, V. S., Tsyro, S., Tuovinen, J. P., Valdebenito, Á., and Wind, P.: The EMEP MSC-W chemical transport model -

technical description, Atmos. Chem. Phys., 12, 7825-7865, 10.5194/acp-12-7825-2012, 2012.
Song, C. H., and G. R. Carmichael, Gas-particle partitioning of nitric acid modulated by alkaline aerosol, J. Atmos. Chem., 40, 1–22, 2001.
Strahan, S. E., Duncan, B. N., and Hoor, P.: Observationally derived transport diagnostics for the lowermost stratosphere and their application to the GMI chemistry and transport model, Atmos. Chem. Phys., 7, 2435-2445, doi:10.5194/acp-7-2435-2007, 2007.
Sudo, K., M. Takahashi, J. Kurokawa, and H. Akimoto, CHASER: A global chemical model of the troposphere, 1. Model description, J. Geophys. Res., 107(D17), 4339, doi:10.1029/2001JD001113, 2002.
Takiguchi, Y., A. Takami, Y. Sadanaga, X. Lun, A. Shimizu, I. Matsui, N. Sugimoto, W. Wang, H. Bandow, and S. Hatakeyama (2008), Transport and transformation of total reactive nitrogen over the East China Sea, J. Geophys. Res., 113, D10306, doi:10.1029/2007JD009462.
Textor, C., Schulz, M., Guibert, S., Kinne, S., Balkanski, Y., Bauer, S., Berntsen, T., Berglen, T., Boucher, O., Chin, M., Dentener, F., Diehl, T., Easter, R., Feichter, H., Fillmore, D., Ghan, S., Ginoux, P., Gong, S., Grini, A., Hendricks, J., Horowitz, L., Huang, P., Isaksen, I., Iversen, I., Kloster, S., Koch, D., Kirkevåg, A., Kristjansson, J. E., Krol, M., Lauer, A., Lamarque, J. F., Liu, X., Montanaro, V., Myhre, G., Penner, J., Pitari, G., Reddy, S., Seland, Ø., Stier, P., Takemura, T., and Tie, X.: Analysis and quantification of the diversities of aerosol life cycles within AeroCom, Atmos. Chem. Phys., 6, 1777–1813, doi:10.5194/acp-6-1777-2006, 2006.
Tost, H., Jöckel, P., Kerkweg, A., Sander, R., and Lelieveld, J.: Technical note: A new comprehensive SCAVenging submodel for global atmospheric chemistry modelling, Atmos. Chem. Phys., 6, 565-574, doi:10.5194/acp-6-565-2006, 2006.
Trail, M., Tsimpidi, A. P., Liu, P., Tsigaridis, K., Rudokas, J., Miller, P., Nenes, A., Hu, Y., and Russell, A. G.: Sensitivity of air quality to potential future climate change and emissions in the United States and major cities, Atmospheric Environment, 94, 552-563, 2014.
Trump, E. R., Fountoukis, C., Donahue, N. M., and Pandis, S. N.: Improvement of simulation of fine inorganic PM levels through better descriptions of coarse particle chemistry, Atmospheric Environment, 102, 274-281, 2015.
Tsigaridis, K., Daskalakis, N., Kanakidou, M., Adams, P. J., Artaxo, P., Bahadur, R., Balkanski, Y., Bauer, S. E., Bellouin, N., Benedetti, A., Bergman, T., Berntsen, T. K., Beukes, J. P., Bian, H., Carslaw, K. S., Chin, M., Curci, G., Diehl, T., Easter, R. C., Ghan, S. J., Gong, S. L., Hodzic, A., Hoyle, C. R., Iversen, T., Jathar, S., Jimenez, J. L., Kaiser, J. W., Kirkevåg, A., Koch, D., Kokkola, H., Lee, Y. H, Lin, G., Liu, X., Luo, G., Ma, X., Mann, G. W., Mihalopoulos, N., Morcrette, J.-J., Müller, J.-F., Myhre, G., Myriokefalitakis, S., Ng, N. L., O'Donnell, D., Penner, J. E., Pozzoli, L., Pringle, K. J., Russell, L. M., Schulz, M., Sciare, J., Seland, Ø., Shindell, D. T., Sillman, S., Skeie, R. B., Spracklen, D., Stavrakou, T., Steenrod, S. D., Takemura, T., Tiitta, P., Tilmes, S., Tost, H., van Noije, T., van Zyl, P. G., von Salzen, K., Yu, F., Wang, Z., Wang, Z., Zaveri, R. A., Zhang, H., Zhang, K., Zhang, Q., and Zhang, X.: The AeroCom evaluation and intercomparison of organic aerosol in global models, Atmos. Chem. Phys., 14, 10845-10895, doi:10.5194/acp-14-10845-2014, 2014.
Tsimpidi, A. P., Karydis, V. A., and Pandis, S. N.: Response of inorganic fine particulate matter to emission changes of sulfur dioxide and ammonia: The eastern United States as a case study, Journal of the Air & Waste Management Association, 57, 1489-1498, 2007.
Tsimpidi, A. P., Karydis, V. A., and Pandis, S. N.: Response of Fine Particulate Matter to Emission Changes of Oxides of Nitrogen and-Anthropogenic Volatile Organic Compounds in the Eastern United States, Journal of the Air & Waste Management Association, 58, 1463-1473, 2008.
Vieno, M., Heal, M. R., Twigg, M. M., MacKenzie, I. A., Braban, C. F., Lingard, J. J. N. Ritchie, S., Beck, R. C., A., M., Ots, R., DiMarco, C. F., Nemitz, E., Sutton, M. A., and Reis, S.: The UK particulate matter air pollution episode of March-April 2014: more than Saharan dust., Environ. Res. Lett., doi:10.1088/1748-9326/11/4/044004, 2016.
Walker, J. M., Philip, S., Martin, R. V., and Seinfeld, J. H.: Simulation of nitrate, sulfate, and ammonium aerosols over the United States, Atmos. Chem. Phys., 12, 11213–11227, doi:10.5194/acp-12-11213-2012, 2012.
Watanabe, S., T. Hajima, K. Sudo, T. Nagashima, T. Takemura, H. Okajima, *et al*. MIROC-ESM 2010: model description and basic results of CMIP5-20c3m experiments, Geosci. Model Dev., 4 (2011), pp. 845–872.

Weber, R. J., Guo, H., Russell, A. G., and Nenes, A.: High aerosol acidity despite declining atmospheric sulfate concentrations over the past 15 years, Nature Geosci., 9, 282-285, 10.1038/ngeo2665, 2016.

Williams, E. J., S. T. Sandholm, J. D. Bradshaw, J. S. Schendel, A. O. Langford, P. K. Quinn, P. J. LeBel, S. A. Vay, P. D. Roberts, R. B. Norton, B. A. Watkins, M. P. Buhr, D. D. Parrish, J. G. Calvert, and F. C. Fehsenfeld, An intercomparison of five ammonia measurement techniques, J. Geophys. Res., Vol., 97, No. D11, Pages 11591-11611, July 20, 1992.

van der Werf, G. R., Randerson, J. T., Giglio, L., Collatz, G. J., Mu, M., Kasibhatla, P. S., Morton, D. C., DeFries, R. S., Jin, Y., and van Leeuwen, T. T.: Global fire emissions and the contribution of deforestation, savanna, forest, agricultural, and peat fires (1997–2009), Atmos. Chem. Phys., 10, 11707-11735, doi:10.5194/acp-10-11707-2010, 2010.

Zender, C. S., Bian, H. S., and Newman, D.: Mineral Dust Entrainment and Deposition (DEAD) model: Description and 1990s dust climatology, J. Geophys. Res.-Atmos., 108, 4416, doi:10.1029/2002jd002775, 2003.

Zhou, J., B. Gu, W. H. Schlesinger, X. Ju, Significant accumulation of nitrate in Chinese semi-humid croplands, Scientific Reports 6, Article number: 25088, doi:10.1038/srep25088, 2016.

Table 1. Nitrate chemical mechanism and physical properties of AeroCom models

Model	CHEM-EQM	HNO3 chem mechanism	CHEM DUST	CHEM SEASALT	How do CHEMDUSS[c]	Bins for nitrate	Model Name & resolution	References
CHASER	ISORROPIA-I	CHASER (Sudo et al., 2002)	No	No	---	Fine mode	MIROC, GCM, 2.8°x2.8°x64	Watanabe et al., 2011
EMAC	ISORROPIA-II (Stable state[a])	MESSy2 (Jöckel et al., 2010)	Yes	Yes	ISORROPIA-II	4 bins: Nucleation, Aitken, Accumulation, Coarse	ECHAM5, GCM, 2.8°x2.8°x31	Karydis et al., 2016
EMEP	MARS	EMEP EmChem09 (Simpson et al., 2012)	Yes	Yes	First order loss	Fine and coarse	ECMWF-IFS, CTM, 0.5x0.5°x20	Simpson et al., 2012
GMI	RPMARES (Stable state)	GMI (Straham et al., 2007)	Yes	Yes	first order loss	3 bins: (D<0.1, 0.1 – 2.5, > 2.5 um)	MERRA2, CTM, 2.5°x2°x72	Bian et al., 2009
INCA	INCA (Stable state)	INCA tropospheric chemistry (Hauglustaine et al., 2004)	Yes	Yes	first order loss	2 bins : (D< 1µm and 1 - 10µm)	LMD-v4, GCM, 1.9°x3.75°x39	Hauglustaine et al., 2014
GISS MATRIX	ISORROPIA-II (Stable state)	MATRIX Bauer (2008) and tropospheric chemistry (Shindell et al., 2003)	No	No	NO	Distributed over all mixing states e.g. size distributions.	NASA GISS-E2, GCM, 2°x2.5°x40	Schmidt et al 2014
GISS OMA	EQSAM_v03d (Metastable[b])	OMA (Bauer 2007) and tropospheric chemistry (Shindell et al., 2003)	Yes	No	Bauer and Koch, 2005	Fine mode	NASA GISS-E2, GCM, 2°x2.5°x40	Schmidt et al 2014
Oslo CTM2	EQSAM_v03d (Metastable)	Oslo CTM2 (Berntsen and Isaksen, 1997)	No	Yes	EQSAM_v03d	2 bins: fine and coarse mode	ECMWF, CTM, 2.8°x2.8°x60	Myhre et al., 2006
Oslo CTM3	EQSAM_v03d (Metastable)	Oslo CTM2 (Berntsen and Isaksen, 1997)	No	Yes	EQSAM_v03d	2 bins: fine and coarse mode	ECMWF, CTM, 2.25°x2.25°x60	Myhre et al., 2006

[a]Stable state: where salts precipitate once the aqueous phase becomes saturated

[b]Metastable: where the aerosol is composed only of a supersaturated aqueous phase

[c]CHEMDUSS: Chemistry reaction on dust and sea salt particles

Table 2. Characteristics of thermodynamic equilibrium models

	ISORROPIA-I	ISORROPIA-II	MARS	RPMARES	INCA	EQSAM_v03d
Species	Sulfate, nitrate, ammonium, sodium, chloride	Sulfate, nitrate, ammonium, sodium, chloride, crustal species	Sulfate, nitrate, ammonium	Sulfate, nitrate, ammonium	Sulfate, nitrate, ammonium	Sulfate, nitrate, ammonium, sodium, chloride
# of components	23	34	16	11	9	18
# of reactions	15	27	7	6	4	25
Multicomponent activity coefficient	Bromley	Bromley	Bromley	Bromley	Seinfeld and Pandis	Metzger
Binary activity coefficient	Kusik and Meissner	Kusik and Meissner	Pitzer	Pitzer	Seinfeld and Pandis	Metzger
Water activity	ZSR[a]	ZSR	ZSR	ZSR		ZSR
Kelvin effect	No	No	No	No	No	No
Quantities that determine subdomains	$[Na^+]$, $[NH_4^+]$, $[SO_4^{2-}]$	$[Ca^{2+}]$, $[K^+]$, $[Mg^{2+}]$, $[Na^+]$, $[NH_4^+]$, $[SO_4^{2-}]$	RH, $[NH_4^+]$, $[SO_4^{2-}]$	$[NH_4^+]$, $[SO_4^{2-}]$	$[NH_4^+]$, $[SO_4^{2-}]$	$[NH_4^+]$, $[SO_4^{2-}]$

# of subdomains	4	5	4	2	3	3

[a]ZSR: *Zdanovskii-Stokes-Robinson*

Table3. Summary of the observational data used in this study

SURFACE NETWORK	QUANTITY	COVER AREA	# of sites in 2008	SAMPLE FREQUENCE	SOURCE
CASTNET	Concentration of HNO_3, NO_3^-, NH_4^+, SO_4^{2-}	North America	83	weekly	www.epa.gov/castnet/clearsession.do
	Dry deposition of them				
AMoN	Concentration of NH_3	U.S.	19	2-weekly	http://nadp.isws.illinois.edu/
NADP/NTN	Wet deposition of HNO_3+NO_3^-, NH_4^+, SO_4^{2-}	U.S.	253	weekly	nadp.isws.illinois.edu
EMEP	Concentration of HNO_3, NH_3, NO_3^-, NH_4^+, SO_4^{2-}	Europe	35	daily	http://www.nilu.no/projects/ccc/index.html
EANET	Concentration of HNO_3, NH_3, NO_3^-, NH_4^+, SO_4^{2-}	East Asia	56	Daily to 2-weekly	http://www.eanet.asia/eanet/brief.html
	Wet deposition of HNO_3+NO_3^-, NH_4^+, SO_4^{2-}			24 hours or precipitation event	
AIRCRAFT CAMPAIGNS	QUANTITY	COVER AREA	# of Flights	CAMPAIGN PERIOD	SOURCE
ARCTAS-A	Concentration of NO_3^-, NH_4^+, SO_4^{2-}	Alaska, U.S.	11	March-April	http://www-air.larc.nasa.gov/cgi-bin/arcstat-c
ARCTAS-CARB		California Bay area U.S.	6	June	
ARCTAS-B		Central Canada	7	July	

Table 4a. NO_3^- global budget for each model

Tracer	Model	Burden (Tg)	SConc (μg kg^{-1})	DDep (Tg a^{-1})	WDep (Tg a^{-1})	ChemDUSS (Tg a^{-1})	ChemP[a] (Tg a^{-1})	Lifetime (days)	AOD[b]
NO_3^-	CHASER	0.16	0.18	-	-	-	-	-	0.0076
	EMAC	0.67	0.47	46.3	-	-		-	-
	EMEP	0.96	0.30	15.0	62.7	(71.7)[c]		4.5	0.0073
	GISS-MATRIX	0.22	0.06	1.3	9.6	(10.9)		7.4	-
	GISS-OMA	0.14	0.05	1.1	5.5	(6.6)		7.8	0.0153
	GMI	0.26	0.22	14.9	31.5	41.9	4.8	2.1	0.0047
	INCA	0.79	0.17	4.5	44.6	44.1	9.8	5.9	0.0064
	Oslo-CTM2	0.60	0.25	47.8	61.5	(109.3)		2.0	0.0018
	Oslo-CTM3	1.88	0.36	34.6	90.6	(125.2)		5.5	-
	Avg	0.63	0.23	20.7	45.9	60.6		5.0	0.0072
	Med	0.60	0.22	15.0	44.6	46.7		5.5	0.0064
	Ratio[d]	13.4	9.4	43.5	16.5	19.0		3.9	8.5

[a]: ChemP refers to NO_3^- chemical production associated with NH_3/NH_4^+

[b]: AOD here includes NH_4^+ that is associated to NO_3^- for all models expect EMEP

[c]: value inside parenthesis is estimated total NO_3^- chemical production based on its total loss, while budget without parenthesis is reported directly by model.

[d]: a ratio between maximum to minimum model simulations

Table 4b NH_3 and NH_4^+ global budget for each model

Tracer	Model	Emi (Tg a^{-1})	Burden (Tg)	SConc (μg kg^{-1})	DDep (Tg a^{-1})	WDep (Tg a^{-1})	ChemP/L[a] (Tg a^{-1})	Lifetime (days)	AOD
NH_4^+	CHASER		0.75	0.44	20.9	7.2	(28.1)[b]	9.8	-
	EMAC		0.19	0.12	3.6	44.5[c]	-	-	-
	EMEP		0.20	0.15	4.0	26.4	(30.4)	2.4	0.0059
	GISS-MATRIX		0.31	0.18	4.1	27.9	(32.0)	3.5	-
	GISS-OMA		0.31	0.19	4.2	24.0	(28.2)	4.0	-
	GMI		0.17	0.14	1.7	30.6	32.2	1.9	-
	INCA		0.39	0.08	2.4	20.4	22.9	6.3	-
	Oslo-CTM2		0.29	0.14	5.3	32.6	(37.9)	2.8	-
	Oslo-CTM3		0.30	0.16	5.6	26.1	(31.7)	3.5	-
	Avg		0.32	0.18	5.8	24.4[d]	30.4	4.3	
	Med		0.30	0.15	4.1	26.3[d]	31.1	3.5	
	Ratio		4.4	5.5	12.3	4.5[c]	1.7	5.2	
NH_3	CHASER	62.8	0.13	0.46	19.8	6.8	(36.2)[b]	0.76	
	EMAC	59.3	0.85	1.39	15.5	-	-	-	
	EMEP	56.9	0.09	0.46	15.4	18.2	(33.6)	0.98	
	GISS-MATRIX	63.4[e]	0.17	0.26	18.1	13.4	(31.9)	0.98	
	GISS-OMA	63.4[e]	0.17	0.25	18.4	16.7	(28.3)	0.98	
	GMI	60.4	0.11	0.40	12.6	17.5	30.4	0.67	
	INCA	70.5[e]	0.12	0.39	29.3	18.6	22.4	0.62	
	Oslo-CTM2	65.9	0.08	0.27	15.8	8.1	(42.0)	0.44	
	Oslo-CTM3	63.3	0.05	0.51	23.7	7.7	(31.9)	0.29	
	Avg	62.9	0.20	0.49	18.7	13.4	32.1	0.72	
	Med	63.3	0.12	0.40	18.1	15.1	31.9	0.72	
	Ratio	1.2	17.0	5.6	2.3	2.7	1.9	3.4	

[a]ChemP/L: chemical production or loss term

[b] chemical budgets inside parenthesis are inferred based on the reported emission and total deposition

[c] EMAC gives total wet deposition of NH_4^+ and NH_3

[d] Statistic values of NH_4^+ wet deposition do not include EMAC

[e] INCA uses ECLIPSE anthropogenic emissions, two GISS models use CMIP5 anthropogenic emission, and all other models use HTAPv2 anthropogenic emissions

Table 4c. HNO_3 global budget for each model

Tracer	Model	Burden[a] (Tg)	SConc (μg kg^{-1})	DDep (Tg a^{-1})	WDep (Tg a^{-1})	CheAP[b] (Tg a^{-1})	CheGP[c] (Tg a^{-1})	CheAL[d] (Tg a^{-1})	CheGL[e] (Tg a^{-1})	Lifetime (days)
HNO_3	CHASER	1.1	0.29	74.0[f]	120.9[f]	-	-	-	-	-
	EMAC	3.1	0.32	56.1	136.0[f]	-	-	-	-	-
	EMEP	0.66	0.04	39.2	123.9	-	-	-	-	-
	GISS-MATRIX	5.7	0.12	61.7	167.5	-	-	-	-	-
	GISS-OMA	5.3	0.10	49.8	148.2	-	-	-	-	-
	GMI	1.8	0.18	39.7	128.1	128.1	413	42.6	299	3.5
	INCA	1.5	0.09	47.7	77.5	21	369	10.0	210	5.7
	Oslo-CTM2	1.3	0.05	36.1	66.0					
	Oslo-CTM3	2.3	0.04	36.0	49.3	-	-	-	-	-
	Avg	2.5	0.14	45.8[g]	108.7[g]					

	Med	1.8	0.10	43.7[g]	123.9[g]
	Ratio	8.6	8.0	1.6[b]	3.4[b]

[a]HNO3 burden for the atmosphere up to 100 hPa
[b]CheAP: chemistry production from aerosol phase
[c]CheGP: chemistry production from gas phase
[d]CheAL: chemistry loss from aerosol phase
[e]CheGL: chemistry loss from gas phase
[f]for both HNO_3 and NO_3^-
[c]statistical values do not include CHASER and EMAC that report total dry or wet deposition of HNO_3 and NO_3^-

Table 4d. SO_4^{2-} global budget for each model

Tracer	Model	Emi SO2 (Tg a^{-1})	Emi SO4 (Tg a^{-1})	Burden (Tg)	SConc (µg kg^{-1})	DDep (Tg a^{-1})	WDep (Tg a^{-1})	Chem GP[a] (Tg a^{-1})	Chem AqP[b] (Tg a^{-1})	Lifetime (days)	AOD
SO_4^{2-}	CHASER	111	0	3.3	1.44	22.1	137	(159)		7.6	0.0826
	EMAC	138	619[c]	1.9	1.72	504[d]	302	(187)		0.86	-
	EMEP	109	0	0.83	0.45	10.2	109	(119)		2.5	0.0232
	GISS-MATRIX	133	5.1	1.3	0.63	16.6	97	(109)		4.2	-
	GISS-OMA	133	5.1	1.1	0.53	11.8	112	52.7	66.2	3.3	0.0714
	GMI	111	0	1.1	0.58	7.5	205	126.5	86.1	3.6	0.0257
	INCA	116.	8.0	1.8	0.34	8.4	116	42.2	75.1	5.3	0.0417
	Oslo-CTM2	133	4.1	2.0	0.49	17.6	184	(198)		3.6	0.0366
	Oslo-CTM3	133	4.1	2.7	0.55	20.2	160	(176)		5.5	
	Avg[e]	122		1.8	0.63	14.3	140	151		4.5	0.0469
	Med[e]	133		1.6	0.54	14.2	127	139		3.9	0.0392
	Ratio[e]	1.2		4.0	4.2	2.9	2.1	2.0		3.0	3.6

[a] ChemGP: Chemistry production from gas phase reaction
[b] ChemAqP: Chemistry production from aqueous phase reaction
[c] EMAC emission also includes sea spray SO_4^{2-}
[d] EMAC dry deposition includes sedimentation and SO_4^{2-} sedimentation is very high since it has assumed that 7.7% of sea salt is SO_4^{2-}
[d] Statistical values do not include EMAC

Table 5: Effective Henry Law constant used in the models

Aerocom Model	$H^{\Theta *}$ (M/atm)	$-\Delta H_{sol}/R$ (K)
CHASER	3.0e+5	3400
EMAC[a]	–	–
EMEP[b]	–	–
GIS MATRIX	1.e+2	3415
GISS OMA	1.e+2	3415
GMI	1.05e6	4200
INCA	7.4e+1	3400
Oslo-CTM2	3.3e+6	0
Oslo-CTM3	3.3e+6	0

[a]EMAC: See its wet deposition description in section 4.1.1.

[b]EMEP: The model does not use Henry law but applies simple empirical scavenging ratio, which for NH_3 is 1.4e6 for in-cloud and 0.5e6 for below-cloud scavenging. The scavenging ratio by definition is the ratio the concentration of a certain pollutant in precipitation divided by the concentration of the pollutant in air.

Table 6. Baseline and three sensitivity experiments in the GMI model

Experiment	Setup	Purpose
BASE	Standard simulation as described in section 2.1	Baseline simulation
TWET	Set NH_3 effective Henry law constant from 1.05e+6 (pH= 5.0) to 62 (pure water)	Review impact of NH_3 wet deposition
TnoNH3	Turn off NO_3^- production from NH_3/NH_4^+	Identify how large/where the NO_3^- formation from NH_3/NH_4^+
TnoHET	Turn off NO_3^- production from dust and sea salt	Identify how large/where the NO_3^- formation from dust and sea salt

Table 7: NO_3^-, NH_4^+, NH_3 and HNO_3 budgets from the base simulation and three sensitivity experiments

Tracer	Exps	Burden (Tg)	SConc (μg kg^{-1})	DDep (Tg a^{-1})	WDep (Tg a^{-1})	ChemDUSS (Tg a^{-1})	ChemP(Tg a^{-1})	Lifetime (days)
NO_3^-	BASE	0.26	0.22	14.9	31.5	41.9	4.8	2.1
	Twet	0.97	0.23	14.8	43.3	41.0	18.3	6.0
	TnoNH3	0.20	0.17	14.7	27.5	42.3	0	1.7
	TnoHET	0.099	0.065	0.61	6.70	0	7.1	5.0

Tracer	Model	Emi (Tg a^{-1})	Burden (Tg)	SConc (μg kg^{-1})	DDep (Tg a^{-1})	WDep (Tg a^{-1})	ChemP/L (Tg a^{-1})	Lifetime (days)
NH_4^+	BASE		0.17	0.14	1.7	30.6	32.2	1.9
	Twet		0.48	0.16	1.9	50.7	53.0	3.4
	TnoNH3		-	-	-	-	-	-
	TnoHET		0.17	0.14	1.6	30.6	32.2	1.9
NH_3	BASE	60.4	0.11	0.40	12.6	17.5	30.4	0.67
	Twet		0.85	0.81	8.70	1.1	50.1	5.2
	TnoNH3		0.32	0.58	20.9	39.3	0	1.9
	TnoHET		0.10	0.40	12.6	17.4	30.4	1.2

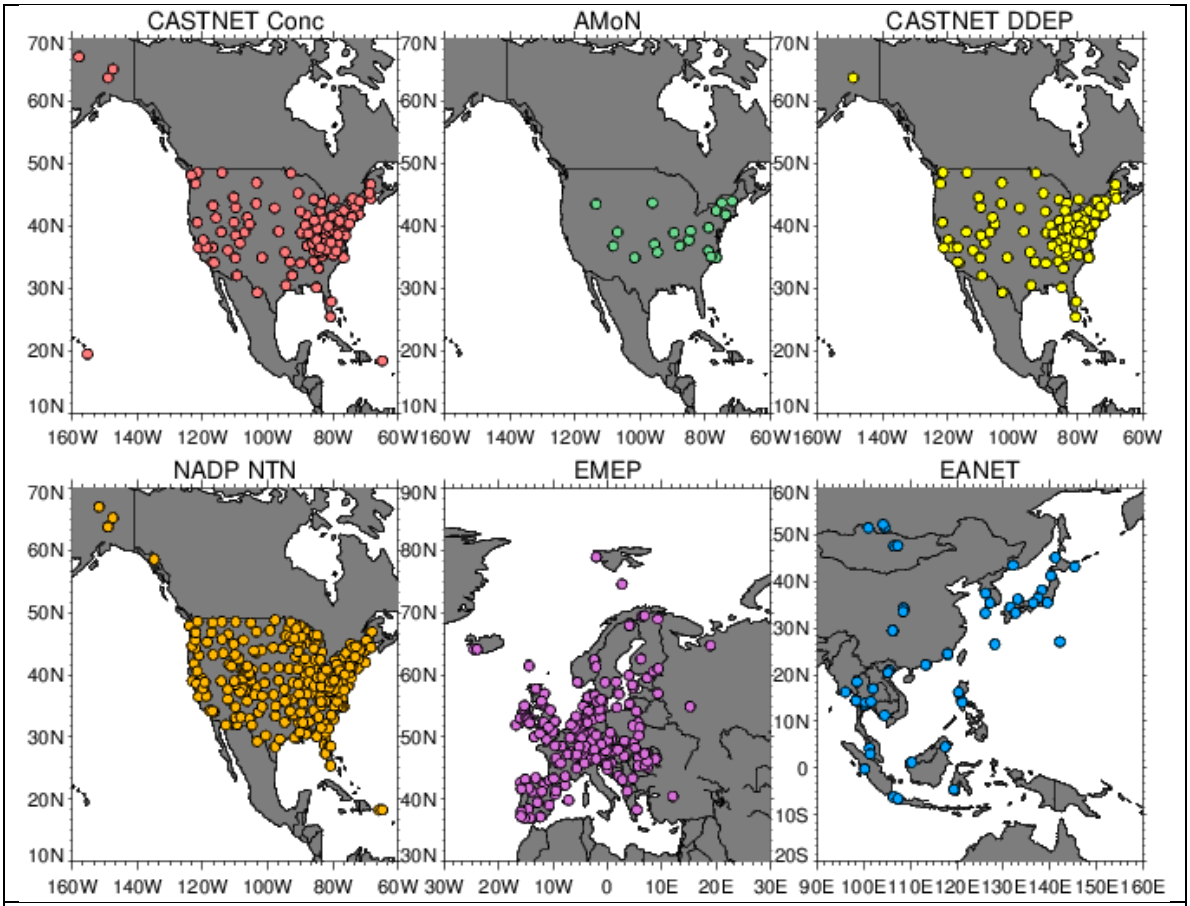

Figure 1. The observational station locations for CASTNET surface concentrations (CASTNET Conc), Ammonia surface monitor network over U.S. (AMON), CASTNET dry deposition (CASTNET DDEP); National Acid Deposition Network for wet deposition over U.S. (NADP NTN), surface concentrations over Europe (EMEP), and surface dry and wet deposition over Asia (EANET).

1306
1307
1308

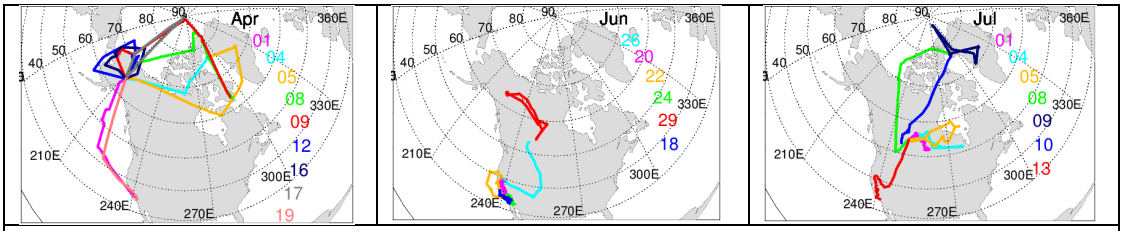

Figure 2. Flight-tracks of ARTCTA-A (left), ARCTAS-CARB (middle), and ARCTAS-B (right). The colors represent observations during different days.

1309

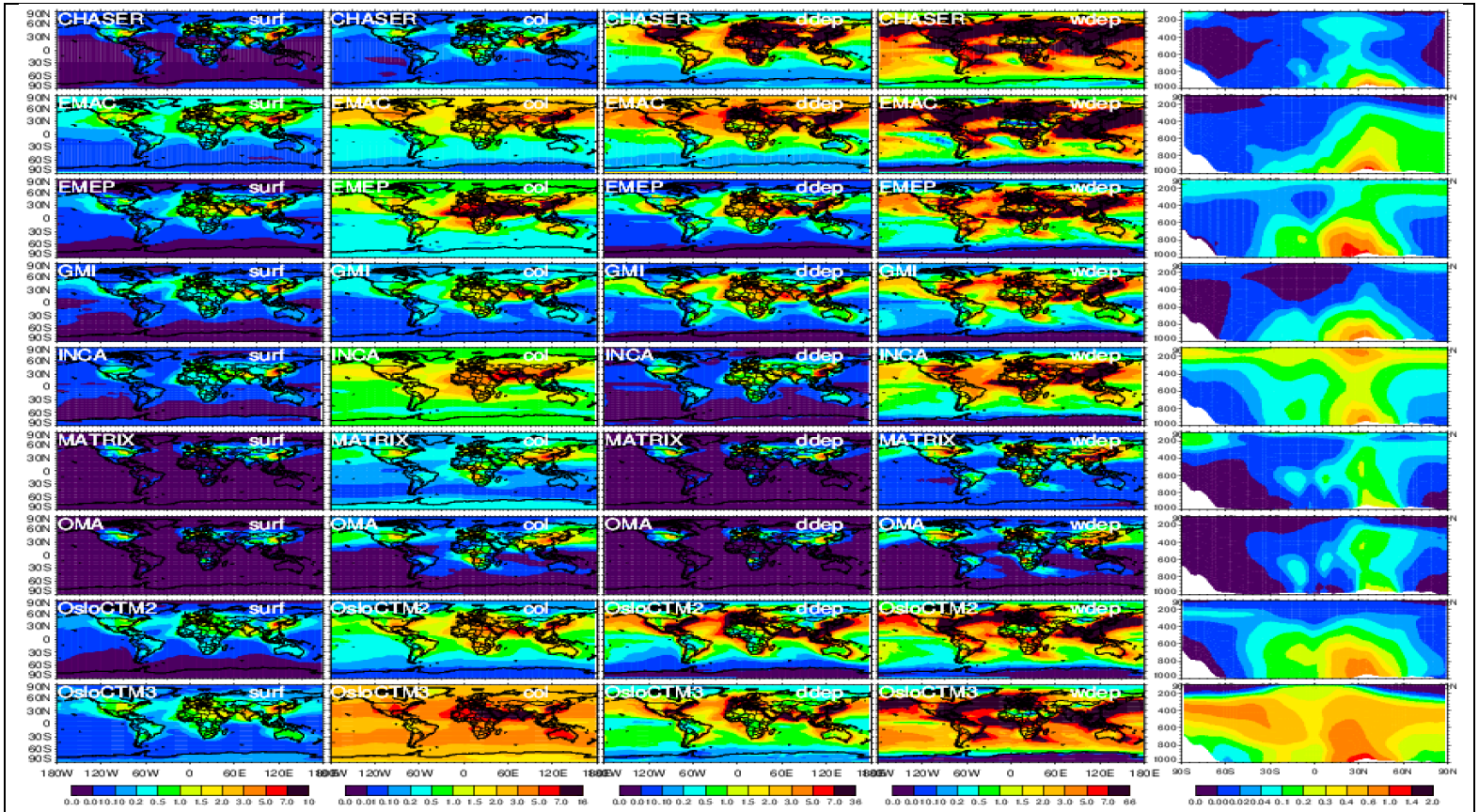

Figure 3a. Multimodel comparison of NO_3^- for surface mass mixing ratio (μg kg^{-1}, left), column load (mg m^{-2}, second), dry deposition (ng m^{-2} s^{-1}, third), wet deposition (ng m^{-2} s^{-1}, fourth), and vertical zonal mean (0.5μg kg^{-1}, right). Note that the CHASER dry and wet depositions and the EMAC wet deposition in this figure contain both NO_3^- and HNO_3, while the rest models NO_3^-.

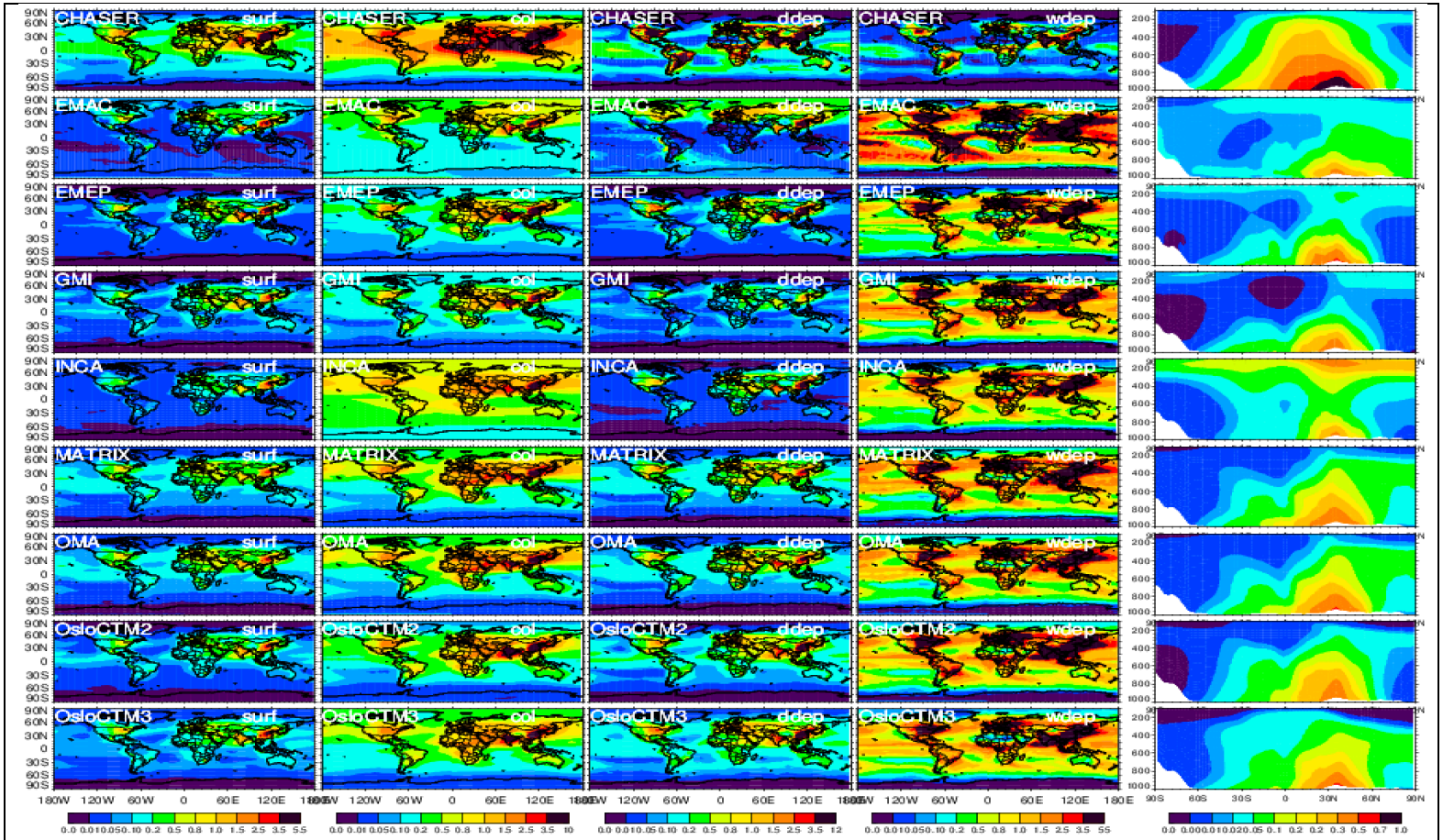

Figure 3b. Same as Figure 3a but for NH_4^+ and the unit in vertical distribution is μg kg^{-1}. Note that the EMAC wet deposition in this figure contain both NH_4^+ and NH_3, while the rest models only NH_4^+.

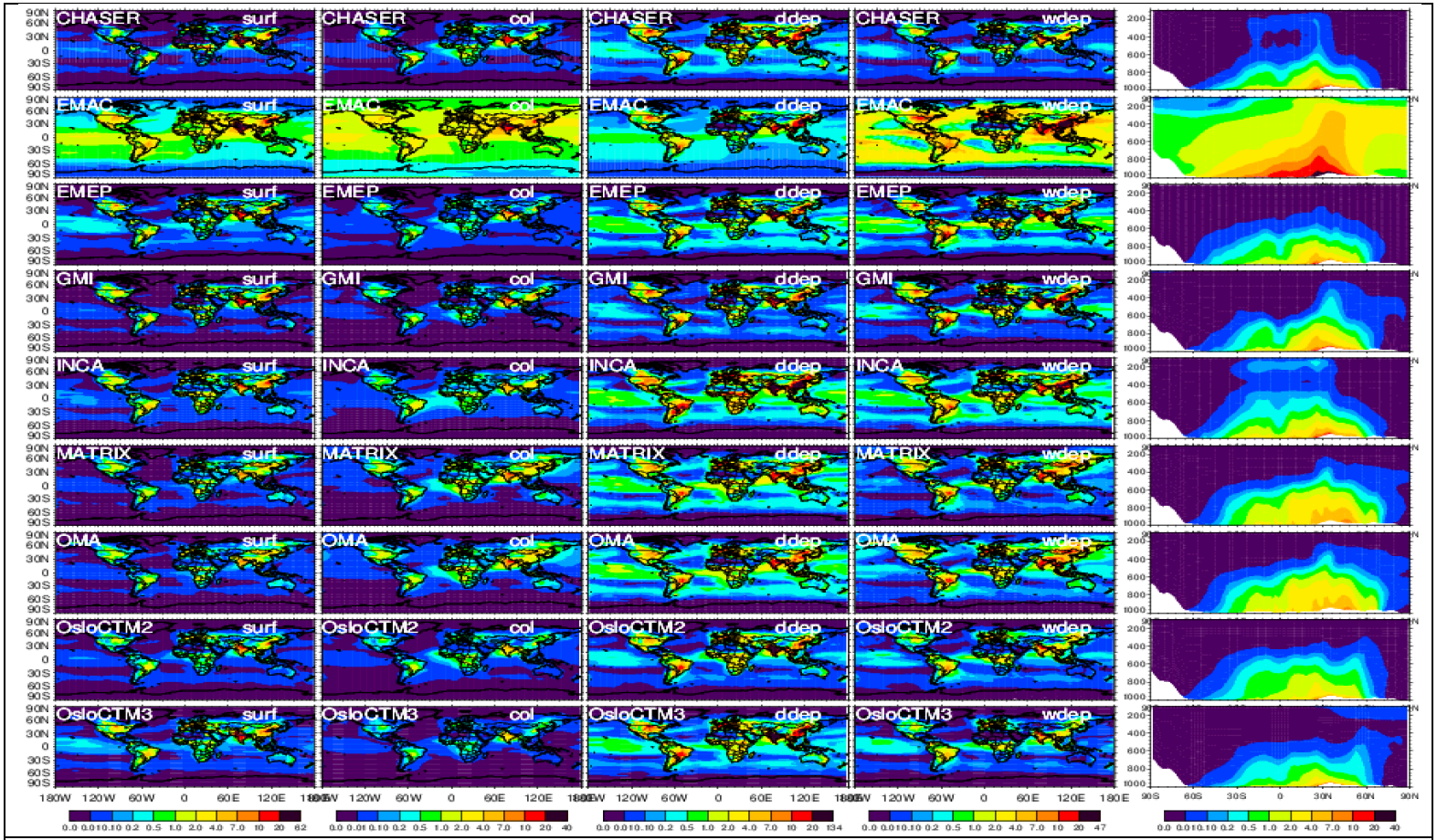

Figure 3c. Same as Figure 3a but for NH_3. Units are ppb for surface concentration and 0.1ppb for vertical distribution. Note that the EMAC wet deposition in this figure contain both NH_3 and NH_4^+, while the rest models only NH_3.

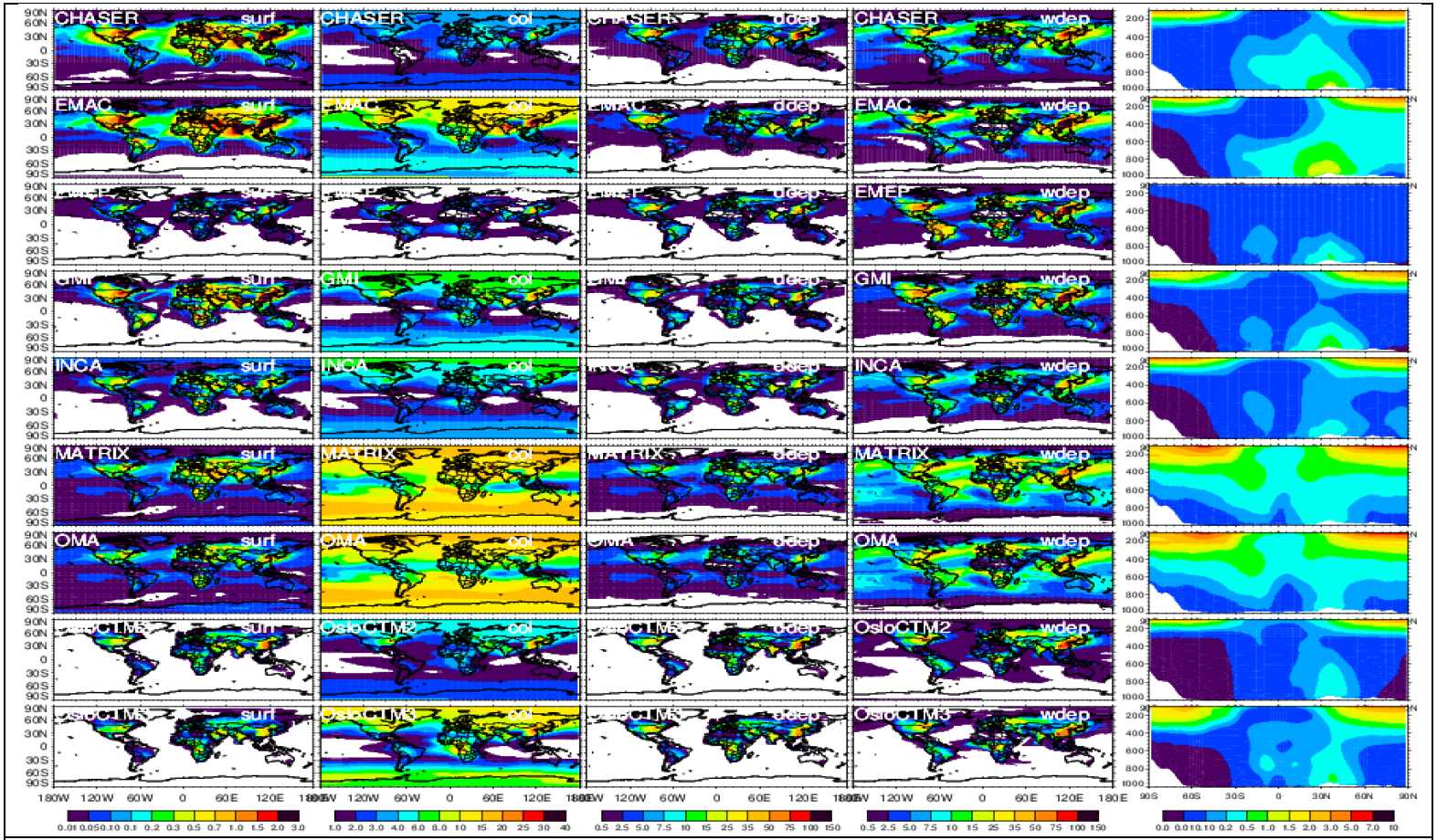

Figure 3d. Same as Figure 3a but for HNO_3. Units are 100 ppb for surface concentration, mg m^{-2} for loading, and 2ng m^{-2} s^{-1} for dry and wet depositions. Note that the column total of HNO_3 is from surface up to 100 ppb vertically. The CHASER dry and wet depositions and the EMAC wet deposition in this figure contain both HNO_3 and NO_3^-, while the rest models only HNO_3.

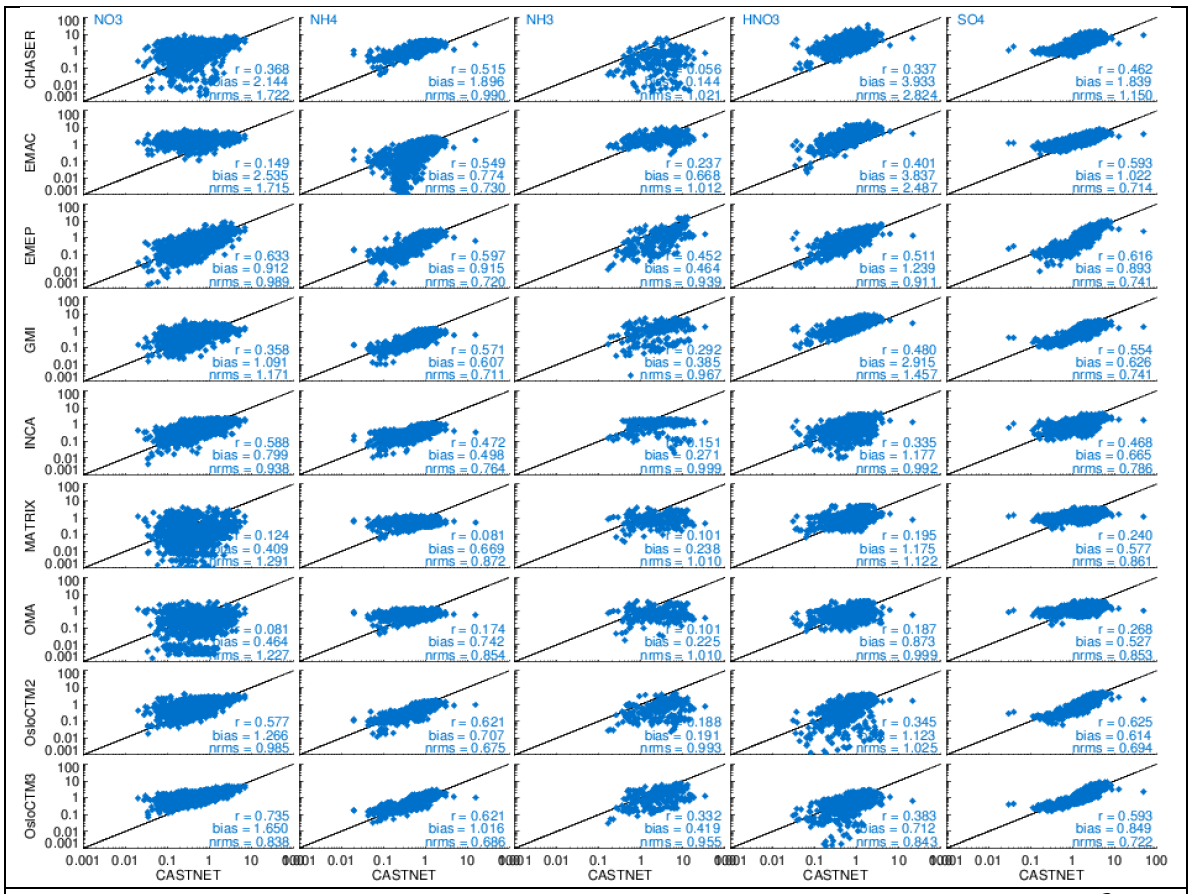

Figure 4a. Comparison of surface mixing ratios of NO_3^-, NH_4^+, NH_3, HNO_3, and SO_4^{2-} between models and CASTNET measurement. Units are μg m^{-3}.

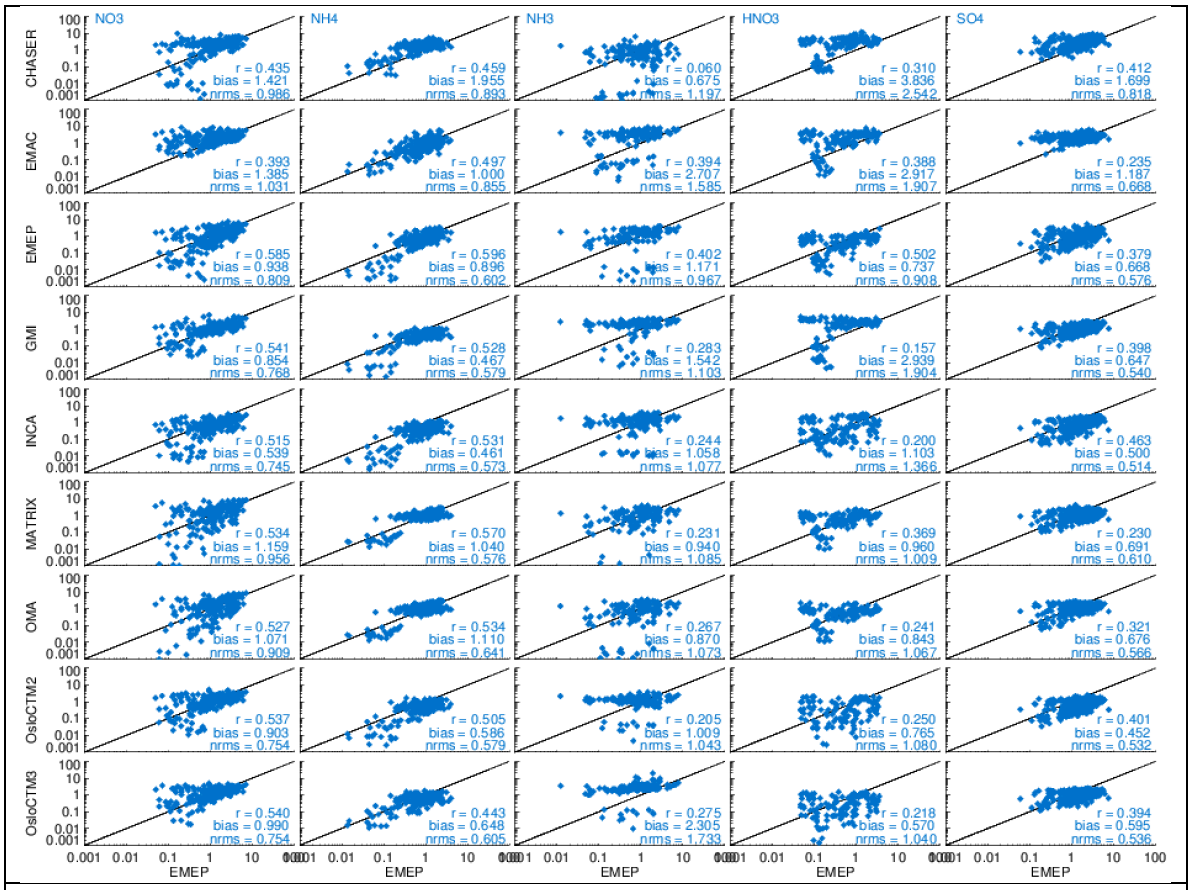

Figure 4b. Same as Figure 4a but for EMEP.

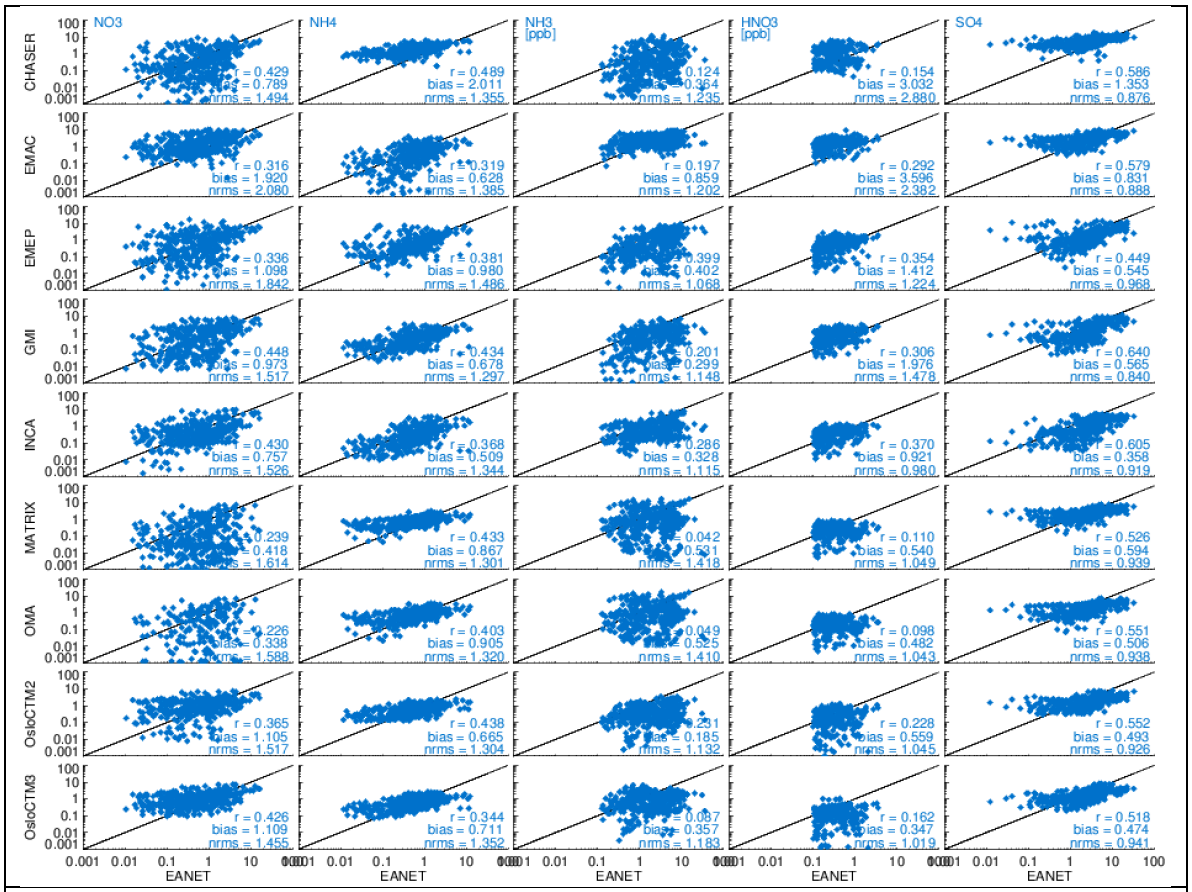

Figure 4c. Same as Figure 4a but for EANET.

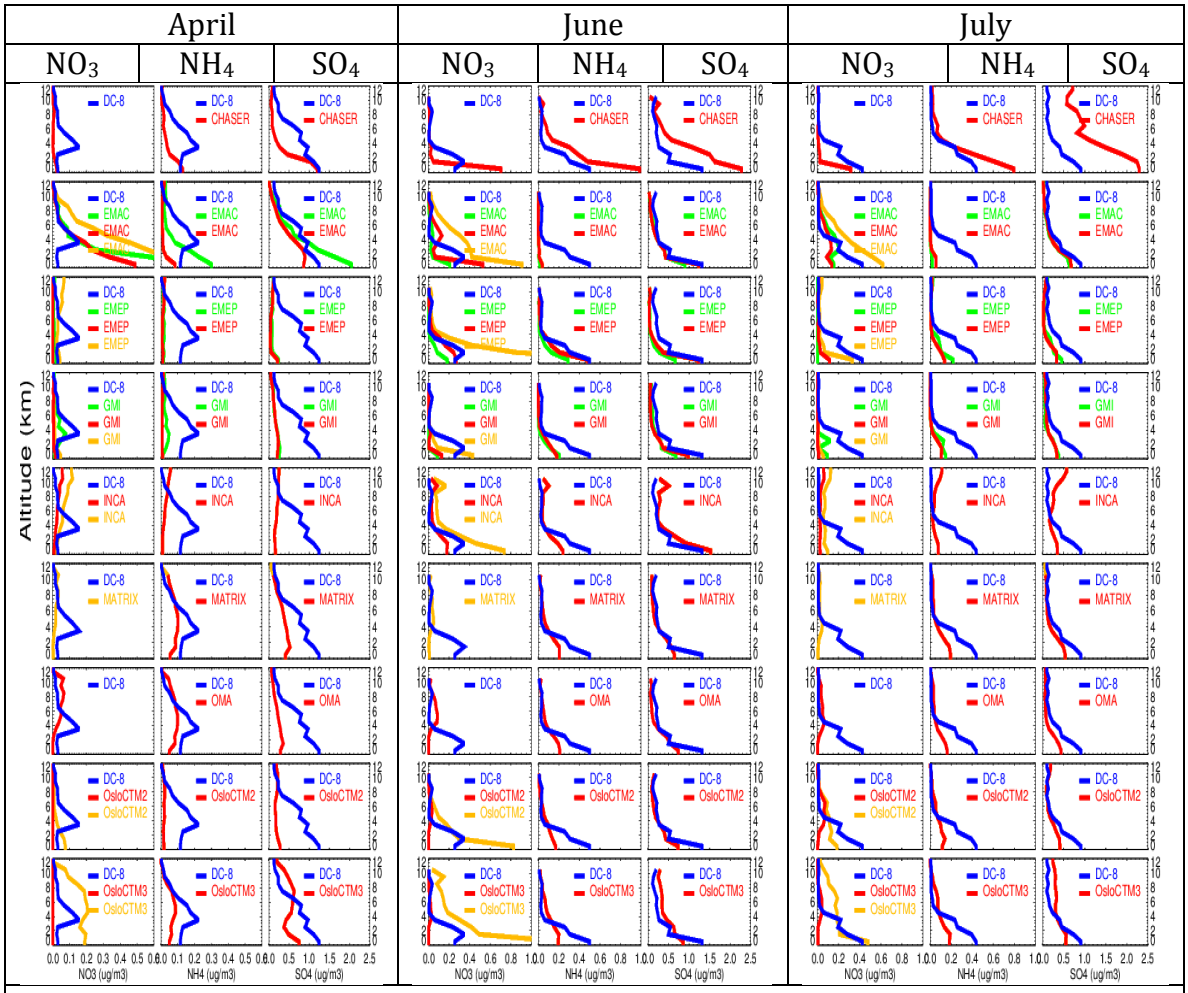

Figure 5. Vertical profile comparison between ARCTAS aircraft measurements and AeroCom model simulations. Note that ARCTAS AMS measurements give fine mode aerosols. Model profiles are shown in green (fine mode aerosol analyzed with daily output), red (fine mode aerosol with monthly output), and orange (total NO_3^- with monthly output). CHASER and OMA have fine mode NO_3^- only. Units are μg m^{-3}.

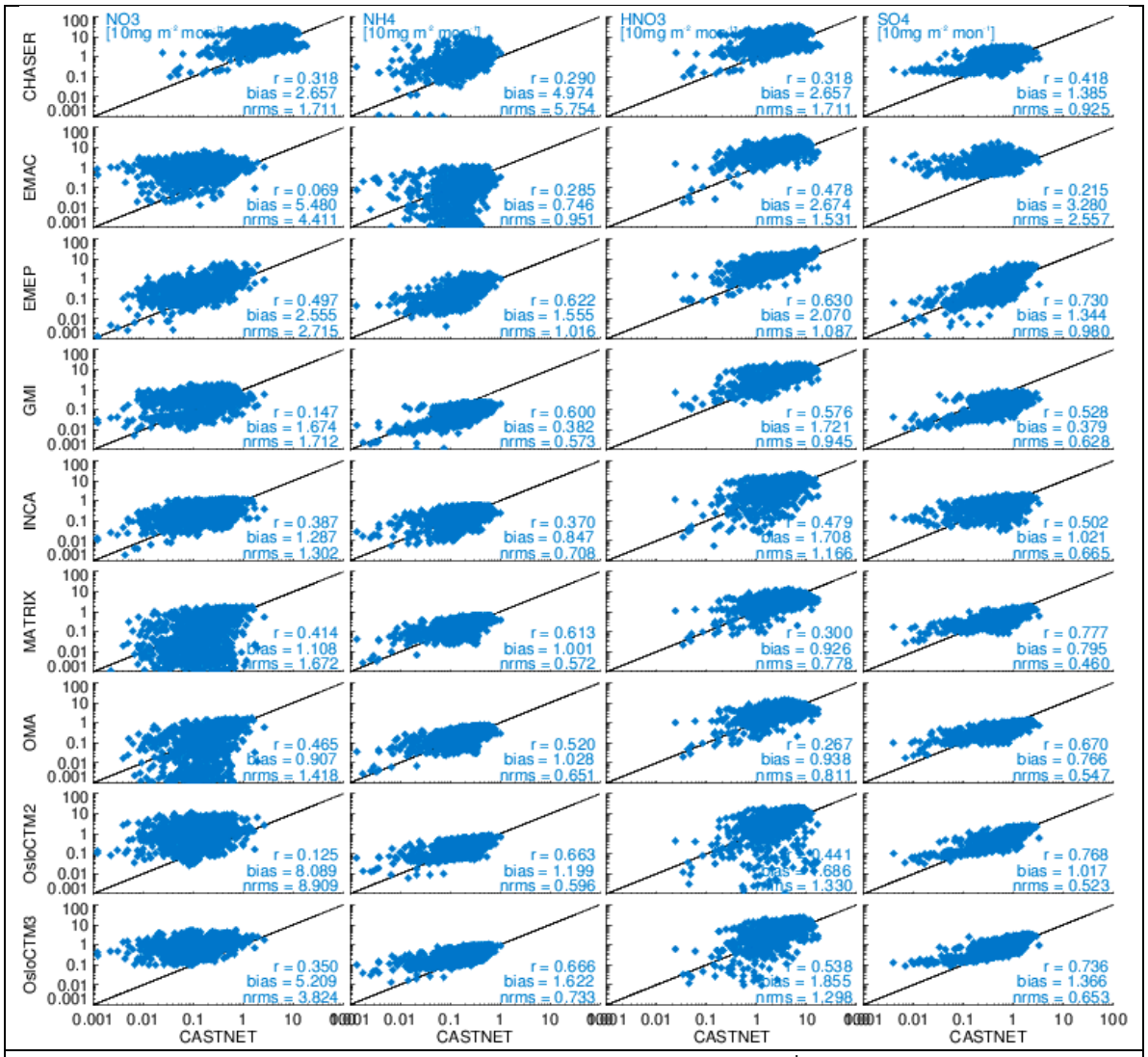

Figure 6. Comparison of surface dry deposition of NO_3^-, NH_4^+, HNO_3, and SO_4^{2-} between models and CASTNET measurements. Units are 10mg m^{-2} mon^{-1}.

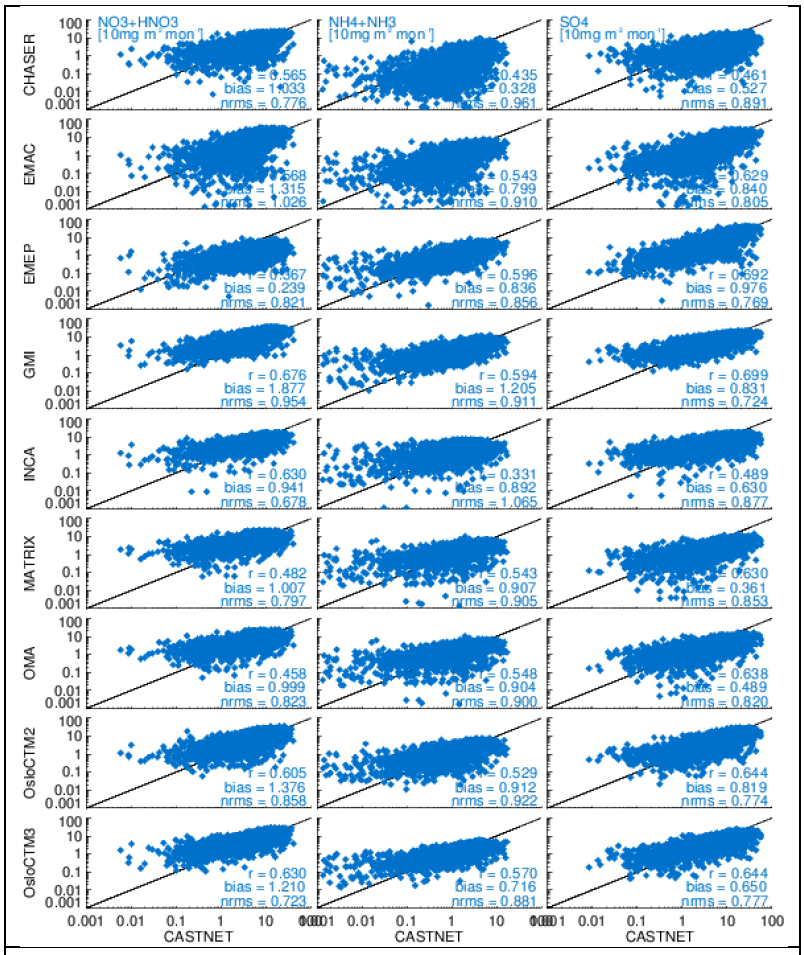

Figure 7a. Comparison of surface wet deposition of NO_3^-+HNO_3, NH_4^++NH_3, and SO_4^{2-} between models and NDAP/NTN measurements. Units are 10mg m^{-2} mon^{-1}.

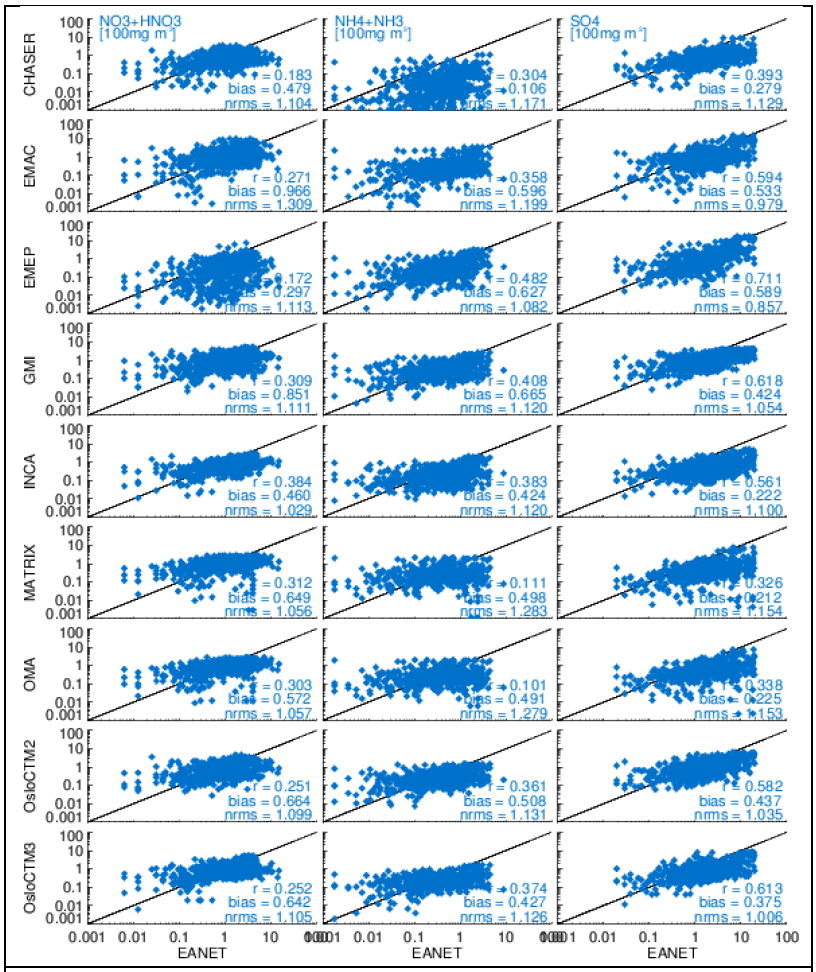

Figure 7b. Same as Figure 7a but for EANET with units of 100mg m^{-3}.

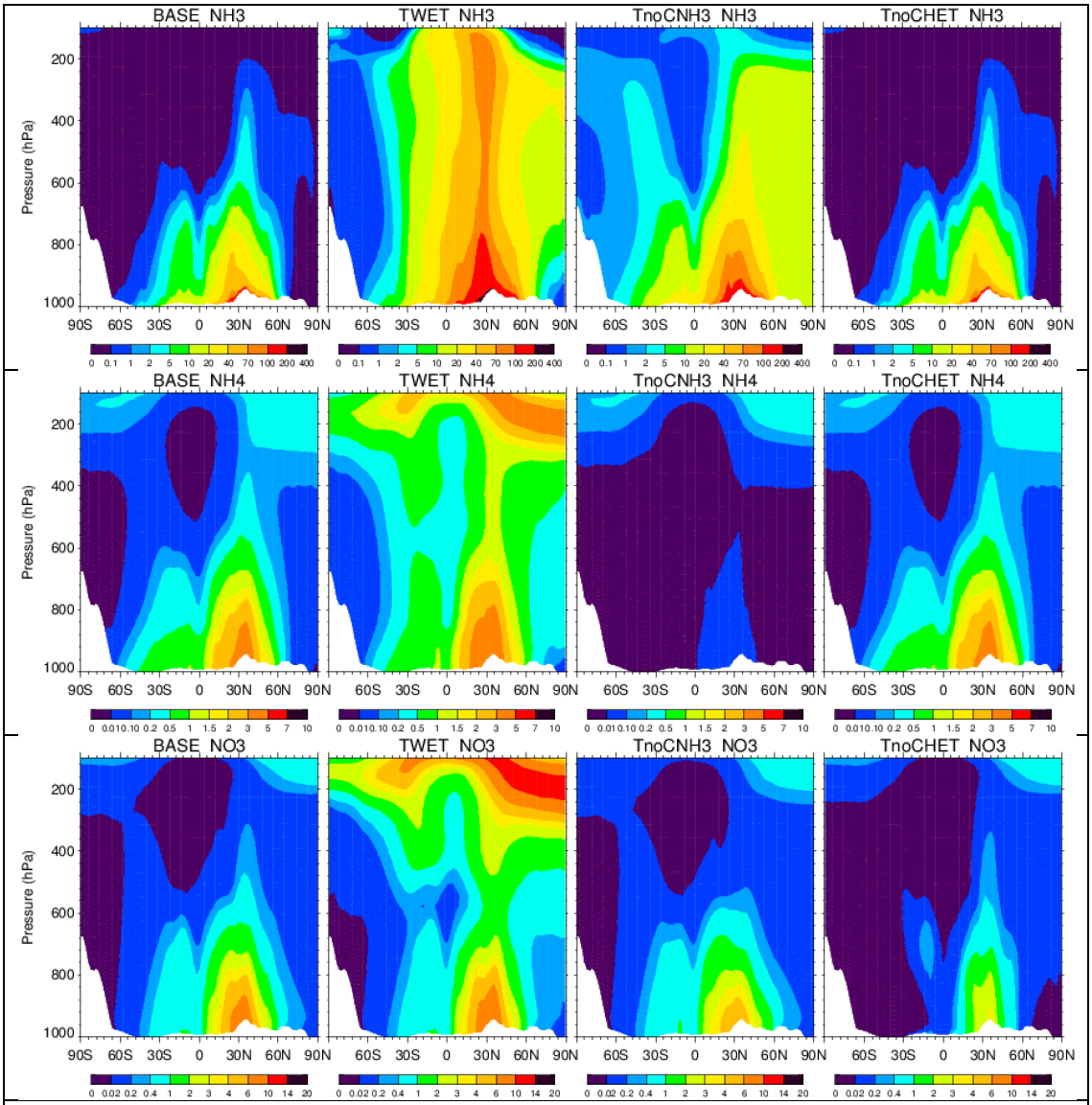

Figure 8. Zonal mean vertical distribution of NH_3 (0.01 ppb), NH_4^+ (0.1 μg kg^{-1}) and NO_3^- (0.05μg kg^{-1}) from base and three sensitivity experiments explained in Table 6.

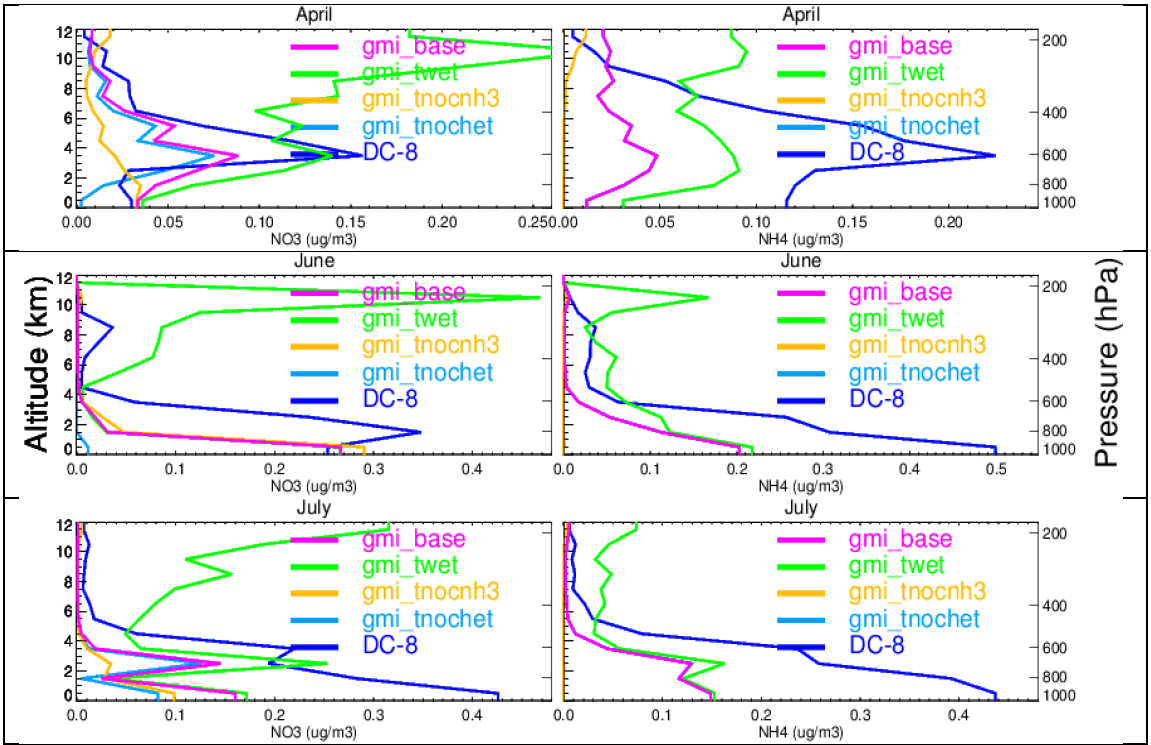

Figure 9. Comparison between GMI simulations and ARCTAS measurements of NH_4^+ and NO_3^- from base and three sensitivity experiments explained in Table 6. Note the light blue line for [NH_4^+] is frequently underneath the peak line.

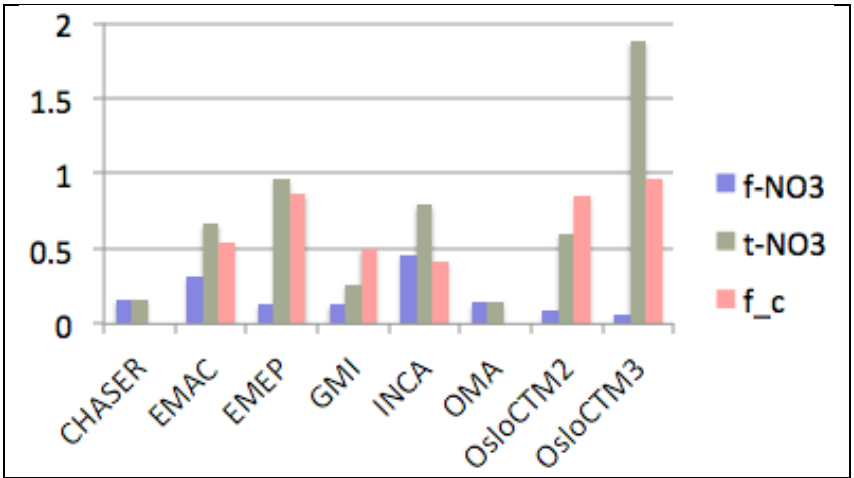

Figure 10. NO_3^- fine mode burden (f-NO3, Tg), total burden (t-NO3, Tg), and coarse mode fraction (f_c) for the eight AeroCom models.